

Benchmarking the CoW with the TopCoW Challenge: Topology-Aware Anatomical Segmentation of the Circle of Willis for CTA and MRA

Kaiyuan Yang^{a,*}, Fabio Musio^{a,b,*}, Yihui Ma^{c,d,*}, Norman Juchler^b, Johannes C. Paetzold^{e,f}, Rami Al-Maskari^f, Luciano Höher^f, Hongwei Bran Li^{a,g}, Ibrahim Ethem Hamamci^a, Anjany Sekuboyina^a, Suprosanna Shit^{a,h}, Houjing Huang^a, Chinmay Prabhakar^a, Ezequiel de la Rosa^a, Diana Waldmannstetter^{a,i}, Florian Kofler^{h,i,j}, Fernando Navarro^{h,i}, Martin Menten^{i,e}, Ivan Ezhovⁱ, Daniel Rueckert^{i,c}, Iris Vos^k, Ynte Ruigrok^l, Birgitta Velthuis^m, Hugo Kuijff^k, Julien Hämmerli^{n,†}, Catherine Wurster^{n,†}, Philippe Bijlenga^{n,†}, Laura Westphal^{o,†}, Jeroen Bisschop^{p,†}, Elisa Colombo^{q,†}, Hakim Baazaoui^{o,†}, Andrew Makmur^{r,†}, James Hallinan^{r,†}, Bene Wiestler^{h,†}, Jan S. Kirschke^{h,†}, Roland Wiest^{s,†}, Emmanuel Montagnon^{t,#}, Laurent Letourneau-Guillon^{t,#}, Adrian Galdran^{u,#}, Francesco Galati^{v,#}, Daniele Falcetta^{v,#}, Maria A. Zuluaga^{v,#}, Chaolong Lin^{w,#}, Haoran Zhao^{w,#}, Zehan Zhang^{x,#}, Sinyoung Ra^{y,#}, Jongyun Hwang^{y,#}, Hyunjin Park^{z,#}, Junqiang Chen^{aa,#}, Marek Wodzinski^{ab,ac,#}, Henning Müller^{ab,#}, Pengcheng Shi^{ad,#}, Wei Liu^{ad,#}, Ting Ma^{ad,ae,#}, Cansu Yalçin^{af,#}, Rachika E. Hamadache^{af,#}, Joaquim Salvi^{af,#}, Xavier Llado^{af,#}, Uma Maria Lal-Trehan Estrada^{af,#}, Valeriia Abramova^{af,#}, Luca Giancardo^{ag,#}, Arnau Oliver^{af,#}, Jialu Liu^{ah,ai,#}, Haibin Huang^{ah,ai,#}, Yue Cui^{ah,ai,#}, Zehang Lin^{aj,#}, Yusheng Liu^{ak,#}, Shunzhi Zhu^{aj,#}, Tatsat R. Patel^{al,am,an,#}, Vincent M. Tutino^{al,am,an,ao,#}, Maysam Orouskhani^{ap,#}, Huayu Wang^{ap,#}, Mahmud Mossa-Basha^{ap,#}, Chengcheng Zhu^{ap,#}, Maximilian R. Rokuss^{aq,ar,#}, Yannick Kirchoff^{aq,ar,at,#}, Nico Disch^{aq,ar,at,#}, Julius Holzschuh^{aq,#}, Fabian Isensee^{aq,as,#}, Klaus Maier-Hein^{aq,au,#}, Yuki Sato^{av,#}, Sven Hirsch^{b,**}, Susanne Wegener^{o,**}, Bjoern Menze^{a,**}

^a Department of Quantitative Biomedicine, University of Zurich, Zurich, Switzerland

^b Center for Computational Health, Zurich University of Applied Sciences, Zurich, Switzerland

^c Department of Neuroradiology, University Hospital of Zurich, Zurich, Switzerland

^d Department of Neurosurgery, Zhongnan Hospital of Wuhan University, Wuhan, China

^e Department of Computing, Imperial College London, London, UK

^f Institute for Tissue Engineering and Regenerative Medicine (iTERM), Helmholtz Center, Munich, Germany

^g Athinoula A. Martinos Center for Biomedical Imaging, Harvard Medical School, Boston, USA

^h School of Medicine, Technical University of Munich, Munich, Germany

ⁱ Department of Informatics, Technical University of Munich, Munich, Germany

^j Helmholtz AI, Helmholtz Munich, Munich, Germany

^k Image Sciences Institute, UMC Utrecht, Utrecht, the Netherlands

^l Department of Neurology, UMC Utrecht, Utrecht, the Netherlands

^m Department of Radiology, UMC Utrecht, Utrecht, the Netherlands

ⁿ Department of Clinical Neurosciences, Division of Neurosurgery, Geneva University Hospitals, Geneva, Switzerland

^o Department of Neurology, University Hospital of Zurich, Zurich, Switzerland

^p Department of Physiology, University of Toronto, Toronto, Canada

^q Department of Neurosurgery, University Hospital of Zurich, Zurich, Switzerland

^r Department of Diagnostic Imaging, National University Hospital, Singapore

^s Department of Diagnostic and Interventional Neuroradiology, University Hospital Berne and University of Berne, Berne, Switzerland

^t Centre de Recherche du Centre Hospitalier de l'Université de Montreal (CRCHUM), Montreal, Canada

^u Universitat Pompeu Fabra, Barcelona, Spain

^v EURECOM, Biot, France

^w Institute of Medical Technology, Peking University Health Science Center, Beijing, China

^x Hangzhou Genlight Medtech Co. Ltd., Hangzhou, China

^y Department of Artificial Intelligence, Sungkyunkwan University, Seoul, Korea

^z Department of Electrical and Computer Engineering, Sungkyunkwan University, Seoul, Korea

^{aa} Shanghai MediWorks Precision Instruments Co., Ltd, Shanghai, China

^{ab} Institute of Informatics, HES-SO Valais-Wallis, Switzerland

^{ac} Department of Measurement and Electronics, AGH University of Krakow, Poland

^{ad} Electronic & Information Engineering School, Harbin Institute of Technology (Shenzhen), Shenzhen, China

^{ae} Peng Cheng Laboratory, Shenzhen, China

^{af} Research Institute of Computer Vision and Robotics (ViCOROB), Universitat de Girona, Catalonia, Spain

^{ag} Center for Precision Health, McWilliams School of Biomedical Informatics, University of Texas Health Science Center at Houston, Houston, USA

^{ah} Laboratory of Brain Atlas and Brain-inspired Intelligence, Institute of Automation, Chinese Academy of Sciences, Beijing, China

^{ai} School of Artificial Intelligence, University of Chinese Academy of Sciences, Beijing, China

^{aj} School of Computer and Information Engineering, Xiamen University of Technology, Xiamen, China

^{ak} Department of Automation, Shanghai Jiao Tong University, Shanghai, China

^{al} Canon Stroke and Vascular Research Center, Buffalo, USA

*K.Y., F.M. and Y.M. contributed equally.

**S.H., S.W. and B.M. are co-corresponding authors.

e-mail: hirc@zhaw.ch (Sven Hirsch), susanne.wegener@usz.ch (Susanne Wegener), bjoern.menze@uzh.ch (Bjoern Menze)

†Clinical committee

#Participant of the challenge, ordered alphabetically by team name

^{am} Department of Pathology and Anatomical Sciences, University at Buffalo, Buffalo, USA

^{an} Department of Neurosurgery, University at Buffalo, Buffalo, USA

^{ao} Department of Biomedical Engineering, University at Buffalo, Buffalo, USA

^{ap} Department of Radiology, University of Washington, Seattle, USA

^{aq} German Cancer Research Center (DKFZ) Heidelberg, Division of Medical Image Computing, Germany

^{ar} Faculty of Mathematics and Computer Science, Heidelberg University, Germany

^{as} Helmholtz Imaging, German Cancer Research Center, Heidelberg, Germany

^{at} HIDSS4Health - Helmholtz Information and Data Science School for Health, Karlsruhe/Heidelberg, Germany

^{au} Pattern Analysis and Learning Group, Department of Radiation Oncology, Heidelberg University Hospital

^{av} LPIXEL Inc., Tokyo, Japan

ARTICLE INFO

Article history:

Keywords: Circle of Willis, Vessel Segmentation, Brain CT Angiography, Brain MR Angiography, Virtual Reality, Vascular Topology

ABSTRACT

The Circle of Willis (CoW) is an important network of arteries connecting major circulations of the brain. Its vascular architecture is believed to affect the risk, severity, and clinical outcome of serious neuro-vascular diseases. However, characterizing the highly variable CoW anatomy is still a manual and time-consuming expert task. The CoW is usually imaged by two angiographic imaging modalities, magnetic resonance angiography (MRA) and computed tomography angiography (CTA), but there exist limited public datasets with annotations on CoW anatomy, especially for CTA. Therefore we organized the TopCoW Challenge in 2023 with the release of an annotated CoW dataset. The TopCoW dataset was the first public dataset with voxel-level annotations for thirteen possible CoW vessel components, enabled by virtual-reality (VR) technology. It was also the first large dataset with paired MRA and CTA from the same patients. TopCoW challenge formalized the CoW characterization problem as a multi-class anatomical segmentation task with an emphasis on topological metrics. We invited submissions worldwide for the CoW segmentation task, which attracted over 140 registered participants from four continents. The top performing teams managed to segment many CoW components to Dice scores around 90%, but with lower scores for communicating arteries and rare variants. There were also topological mistakes for predictions with high Dice scores. Additional topological analysis revealed further areas for improvement in detecting certain CoW components and matching CoW variant topology accurately. TopCoW represented a first attempt at benchmarking the CoW anatomical segmentation task for MRA and CTA, both morphologically and topologically.

1. Introduction

The Circle of Willis (CoW) is an important anastomotic network of arteries connecting the anterior and posterior circulations of the brain, as well as the left and right cerebral hemispheres (Osborn, 2013). Due to its centrality, the CoW is commonly involved in pathologies like aneurysms and stroke. Clinically, the vascular architecture of the CoW is believed to impact the occurrence and severity of stroke (Chuang *et al.*, 2013; van Seeters *et al.*, 2015; Kim *et al.*, 2016), pose a potential risk for aneurysm formation (Rinaldo *et al.*, 2016), and affect the neurologic events and clinical outcomes of neuro-surgeries (Yang *et al.*, 2017; Banga *et al.*, 2018). An accurate characterization of the CoW is therefore of great clinical relevance.

However, clinicians have articulated an unmet demand for efficient software tools to analyze and compare the angio-architecture of the CoW. Assessing the anatomy and vascular components of the CoW from angiography images is still an expert task and time-consuming. The anatomy of the CoW involves multiple joining and branching of different cerebral ves-

sels of various dimensions, with diameters from around 1 to 4 mm (Krabbe-Hartkamp *et al.*, 1998). CoW vessel components are hard to identify accurately in isolation and often require subtle spatial relationship to tell them apart anatomically. The vessels also have curvatures and turns along their courses. This can result in vessels crossing paths on the angiography images but can be difficult to differentiate whether the vessels are just touching or there are communicating blood flows at the crossing points. Furthermore, the CoW naturally has many variants of which certain principal artery components are hypoplastic or absent. It is estimated that only less than around half of our population has a complete CoW (Krabbe-Hartkamp *et al.*, 1998; Iqbal, 2013). It is common to see the CoW anatomies vary markedly from person to person. Thus characterizing the CoW anatomies can be a challenging task both clinically due to the complex anatomy and technically due to the heterogeneity of the data.

Commonly the brain arteries including the CoW are diagnosed and imaged by two angiographic imaging modalities, namely magnetic resonance angiography (MRA) and computed

tomography angiography (CTA). There have been a few publicly available datasets on MRA modality, such as the CASILab (Bullitt et al., 2005) and the IXI datasets¹, but the MRA scans were acquired from fairly old machines (from the year 2004 to 2006). More importantly, very limited annotations were provided if any. Annotated dataset on the other important modality, CTA, is even rarer. Thus we were motivated to release a recent dataset of joint-modalities, i.e. CTA and MRA of the same patients, and with annotations of the underlying CoW anatomy.

Previously there has been a high barrier to entry for annotating the CoW anatomy: one would not only need to overcome the tedious and (very) time-consuming vessel annotation process in 2D for the many CoW vessel labels, but also to get expert neurological and neurosurgical knowledge to label or verify the complex and highly heterogeneous CoW vascular network. To address such obstacles in data annotation, we turned to virtual reality (VR) to significantly speed up the annotation and verification process in 3D (Kaltenecker et al., 2024), and to attract clinicians' interest and domain expertise via VR's powerful visualization and gamification aspects.

Prior work on the CoW anatomy characterization task has been developed mainly as a labelling task built upon binary vessel masks, skeletons or graphs (Bogunović et al., 2013; Robben et al., 2013, 2016; Chen et al., 2020; Hong et al., 2023), and with one recent work that directly tackled the problem as a multiclass segmentation task (Dumais et al., 2022). However, only private annotated in-house data or public data without verified CoW annotations were used, and the studies were restricted to only the MRA modality. Furthermore, given the complex and highly heterogeneous anatomies of the CoW variants in real-life, the difficulties and pain points of the CoW anatomy characterization task in past studies have not been sufficiently conveyed or discussed. We thus identify the following contributions we can make to the field: 1) Open data with verified annotations for CoW segmentation benchmarking. A public annotated CoW dataset can benefit algorithm development and comparison. 2) Inclusion of the CTA modality. Clinically, CTA is an equally important angiography modality as MRA for CoW anatomy diagnosis. With paired CTA and MRA of the same patients available, we also have higher confidence in the accuracy of our CoW anatomical labels and variant diagnosis. 3) Shed light on the complexity from CoW variants. The released dataset and annotations cover and categorize clinically representative anterior and posterior CoW variants. We also introduce metrics and analysis focusing on the CoW variant and its topology to capture the clinical relevance.

To fill the research gap in good quality CoW anatomical annotations, newer imaging datasets of paired modalities, and a benchmark for CoW segmentations, we organized the challenge called “**Topology-Aware Anatomical Segmentation of the Circle of Willis for CTA and MRA**”, or **TopCoW** for short, as registered and included in the Medical Image Computing and Computer Assisted Intervention (MICCAI) conference held in Vancouver Canada 2023. TopCoW was the first public challenge on CoW anatomical segmentation with voxel-level ves-

sel annotations on two common angiographic imaging modalities, MRA and CTA. The aim of the challenge was to automatically segment the CoW vessels from 3D angiographic imaging. There were two segmentation tasks: a multiclass segmentation task for thirteen possible CoW vessel components, and a binary segmentation task for the combined CoW vessel class. There were also two tracks for participants to choose from, one track for each imaging modality. A technical emphasis of this challenge was on topology-aware segmentation. The segmented vessels should retain the topology of the underlying anatomy. We evaluated the segmentation performance on both overlap-based and topology-based metrics such as connected components and centerlines (Shit et al., 2021; Stucki et al., 2023; Menten et al., 2023). Additional topological analysis on the detection and topology matching aspects were also performed.

In this paper, we first describe our TopCoW challenge dataset and present the dataset properties in Section 2. We then give an overview of the TopCoW challenge setup and evaluation methods in Section 3. We summarize the submitted methods and their performance on our testset as a first attempt at benchmarking the CoW anatomical segmentation tasks, both morphologically and topologically, in Section 4. Lastly, we discuss winning algorithm designs, open problems, and future tasks in Section 5.

2. TopCoW Challenge Dataset and Analysis

In this section, we comprehensively document the properties of the TopCoW challenge dataset and the annotation protocol. We also provide the analysis on the data and annotation characteristics such as exclusions of certain CoW variants, inter-rater agreement, inter-modality agreement, and the CoW variant distribution in our data.

2.1. Challenge Data Cohort

The challenge data cohort was composed of patients admitted to the Stroke Center of the University Hospital Zurich (USZ) in 2018 and 2019. The inclusion criteria for the challenge data were: 1) both MRA and CTA scans were available for that patient; 2) at least the MRA or CTA allowed for an assessment of the CoW anatomy. The patients of the challenge cohort were admitted for or recovering from a stroke-related neurological disorder, including ischemic stroke, transient ischemic attack, stroke mimic, retinal infarct or amaurosis fugax, intracerebral hemorrhage, and cerebral sinus vein thrombosis.

2.2. Image Data Acquisition

The MRA and CTA data were typically acquired by various Siemens scanners during routine examinations following standard clinical protocols. MRA scans were imaged with magnetic field strength of 3 Tesla or 1.5 Tesla. Most of the data were acquired at the USZ during routine examinations following standard procedures for MRA and CTA. Some of the data were acquired by neighbouring Swiss hospitals before the patients were transferred to USZ. The dataset can be considered to be multi-site from Switzerland.

¹<https://brain-development.org/ixi-dataset/>

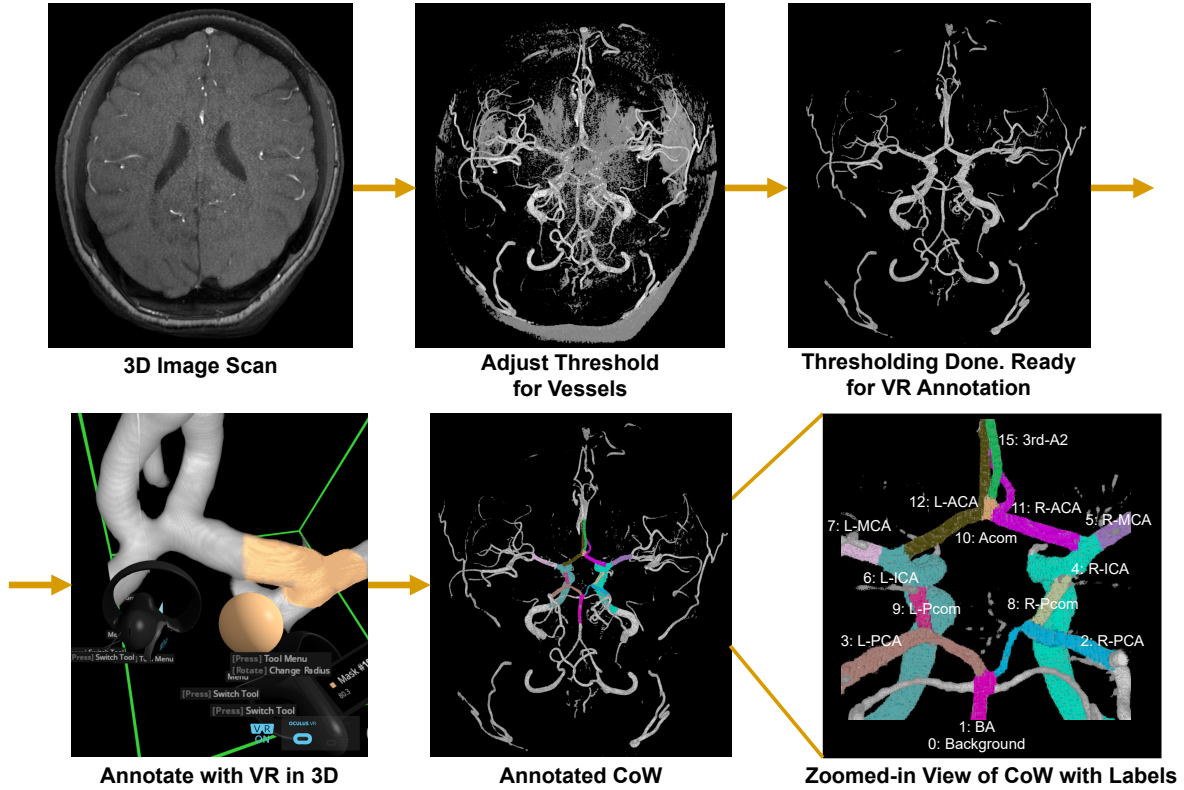


Fig. 1. Data annotation procedure using VR as demonstrated on an example MRA scan. The bottom right image shows the thirteen possible anatomical labels for CoW anatomy as annotated on this MRA scan. Note the view angle is from behind the back and from the head to the feet, thus the left and right sides are not flipped.

2.3. Anonymization and Defacing

The data were anonymized (removal and anonymization of relevant DICOM patient information). Additional de-facing and cropping procedures were performed to ensure patient privacy in the image data after converting the DICOM to NIfTI format using `dcm2niix` (Li et al., 2016). Specifically, we masked out the face using TotalSegmentator (Wasserthal et al., 2023) for CTA modality and shear-cutted the facial regions with quickshear method (Schimke and Hale, 2011) for MRA modality, and then cropped the image data using brain mask from TotalSegmentator for CTA modality or HD-BET (Isensee et al., 2019) for MRA modality. The defaced image included only the braincase region.

2.4. Data Annotation Setup

VR was used to efficiently annotate and verify the CoW anatomy in 3D. Fig. 1 and Fig. 2 show the workflow and view from VR. The software used to visualize VR was `syGlass` (Pidhorskyi et al., 2018). The hardware used was Meta Quest. For more information on the VR annotation setup, please refer to related prior work (Kaltenecker et al., 2024) and the tutorial session organized for ICCV 2023 at <https://xr4biomed.github.io/>.

For each 3D angiography image, we provided two types of annotations: voxel-level multiclass segmentation mask, and a 3D bounding box for the CoW region of interest (ROI). We now describe the two types of annotation in the following subsections.

2.5. Annotation-I: CoW Multiclass Mask

In total we defined thirteen possible CoW vessel component labels. Fig. 1 contains the annotation mask in pixel value for each CoW vessel component for an MRA example. The vessel components of the CoW annotated were left and right internal carotid artery (ICA), left and right anterior cerebral artery (ACA), left and right middle cerebral artery (MCA), anterior communicating artery (Acom), left and right posterior communicating artery (Pcom), left and right posterior cerebral artery (PCA), and basilar artery (BA). Occasionally the anterior part of the CoW can have a third A2 artery arising from the Acom, and we labelled it with class 3rd-A2.

Note that only vessel components and regions necessary to diagnose the CoW angio-architecture and variants were annotated. The voxel annotations covered a larger volume than the CoW ROI, i.e. the voxel annotations extended beyond the ROI. (See below Section 2.6 on CoW ROI for more info.)

2.6. Annotation-II: CoW ROI

The CoW ROI was defined as the 3D bounding box containing the volume required for the diagnosis of the CoW variant. Fig. 2 shows an example CoW ROI for each modality. The annotated CoW ROI bounding box was released for all training and validation cases. The evaluations of segmentation results were limited to within the CoW ROI. In the last three rows of Table 1, we show the statistical summary of the CoW ROI sizes.

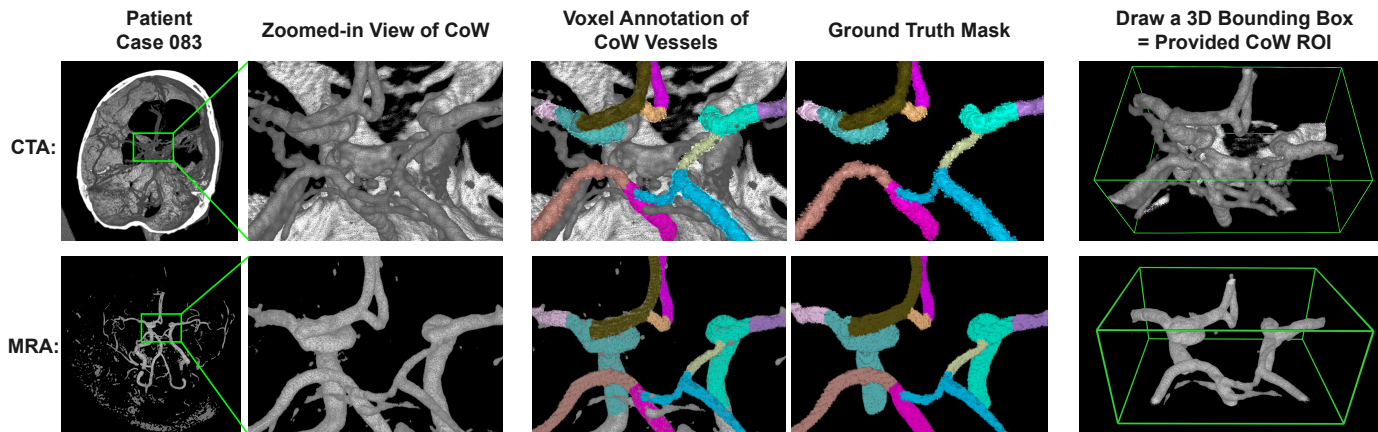


Fig. 2. TopCoW dataset has paired modalities, CTA and MRA, from the same patient. For each modality we provide two types of annotation: voxel annotations of the CoW anatomy and a 3D bounding box for the CoW ROI.

2.7. Annotation & Verification Protocol

Initial CoW annotations were manually labeled voxel-wise as shown in Fig. 1 and Fig. 2, by research staff who had gone through CoW anatomy education from the clinical experts. The cases that annotators were uncertain were flagged, and sent for further verification and approval by the clinical experts. The clinical expert team consisted of neuro-radiologists, neurologists, and neurosurgeons.

All patients from the TopCoW challenge had both CTA and MRA modalities, with one scan for each modality. Annotators and clinical experts had both CTA and MRA modalities available to annotate and verify. The anatomy of the CoW was first inspected in both CTA and MRA to diagnose the anatomical components. Then the CoW vessels were annotated for each modality separately.

The annotation protocol on how to segment vessel components at bifurcation points such as ACA-ICA-MCA, ACA-Acom, PCA-Pcom, Pcom-ICA, etc., were discussed and agreed upon by the clinical experts. For example, we marked the superior tip of the ACA-ICA-MCA bifurcations to be part of ICA, and similarly for BA-PCA bifurcation, we marked the tip to be of BA. We also included the infundibulum as the origin of certain vessel components such as Pcom. The annotation protocol also covered CoW variants such as fetal PCA, triple ACA etc.

For vessels extending beyond the CoW ROI such as the ACA, MCA, and PCA, we typically only labelled until the first major bifurcation occurs, and we only labelled the main vessel instead of any minor branches. For the CTA modality, the ICAs were not labelled through the anterior clinoid and sphenoid bone regions, but were labeled starting from the C7 segment in Bouthillier classification system (Bouthillier et al., 1996). For MRA, we labelled the entire curvature of the ICA in the CoW region even in bone regions.

The qualitative results of our paper show both the source image and the ground truth annotations. These figures aim to display a wide range of CoW variants and in the process give a glimpse into our CoW annotation protocol.

2.8. VR Annotation Speed

Given the relative new adoption of VR in our annotation workflow, here we document the VR annotation speed for the multiclass annotation and drawing of 3D ROI. The preparation steps involved loading the 3D scan and adjusting window and threshold for visualization as Fig. 1 demonstrates. The preparation usually took only a few minutes. The voxel-level annotation for CoW anatomy with VR took around 30–45 minutes. Usually the more CoW vessel components there were, the more time it took to annotate. For example, a CoW without the communicating arteries like Acom and Pcoms would take less time than say, a complete CoW. The annotation time also depended on several other factors, such as whether there were vessels tangled up which made it difficult to label individual segments, or when the tubular structures of the vessels touched and were in close proximity. In CTA scans, there were extra difficulties such as when vessels were mixed with the bone intensities and when veins were mixed with arteries. The 3D bounding box annotation for the CoW ROI was the easiest step and only took one or two minutes. Thus in one hour, the manual annotation for a 3D image scan like in Fig. 1 could be done, or within two hours for a pair of CTA and MRA modalities for a patient such as in Fig. 2.

2.9. Train, Validation, and Test sets

In total 130 pairs of MRA and CTA scans from unique patients were curated for the TopCoW challenge. The split of training, validation, and test sets was by patient and arbitrarily via study IDs. Training, validation, and test cases all had the MRA and CTA joint-modality pairs, with one scan for each modality. Training dataset had 90 patients with the image, segmentation mask, and CoW ROI released. Validation set had 5 patients with image and CoW ROI released to public, but without mask annotations. The small validation set was intended to validate the docker submission technically and not counted towards the ranking. The hidden test set had 35 patients and was not released to the public. In addition to the above TopCoW challenge data, we also released 20 MRAs from the CROWN

Table 1. Data characteristics of the TopCoW training and test sets. Values are shown in mean \pm standard deviation.

	Train (n=90)		Test (n=35)	
	MRA	CTA	MRA	CTA
Pixel Spacing (mm)	0.30 \pm 0.02	0.45 \pm 0.06	0.30 \pm 0.02	0.46 \pm 0.06
Slice Thickness (mm)	0.60 \pm 0.03	0.71 \pm 0.07	0.60 \pm 0.04	0.73 \pm 0.02
Whole image size in X (mm)	143.73 \pm 6.59	136.54 \pm 5.76	144.73 \pm 7.48	137.63 \pm 7.07
Whole image size in Y (mm)	174.02 \pm 8.66	170.35 \pm 9.42	173.09 \pm 8.05	169.96 \pm 9.71
Whole image size in Z (mm)	111.53 \pm 11.07	148.96 \pm 8.87	111.34 \pm 9.81	149.11 \pm 7.86
CoW ROI size in X (mm)	44.90 \pm 3.94	45.51 \pm 4.14	49.06 \pm 4.46	49.63 \pm 4.73
CoW ROI size in Y (mm)	34.78 \pm 3.19	33.51 \pm 3.88	36.25 \pm 3.38	35.75 \pm 3.43
CoW ROI size in Z (mm)	22.23 \pm 3.10	20.92 \pm 3.08	23.44 \pm 3.36	21.38 \pm 3.68

challenge (Vos et al., 2023) with our annotations (multiclass voxel masks and a CoW ROI) for training.

All TopCoW challenge data were anonymized, defaced and cropped to the braincase region (see the previous Section 2.3). Other than the defacing and the cropping to braincase region steps, no further preprocessing of the data was performed to keep the data as close to the clinical setting as possible. The image data were saved in NIfTI format, 16-bit signed, and in LPS+ orientation. The mask data were saved in NIfTI format, 8-bit unsigned, with the same orientation as the source image. The data used in this challenge had been approved by the local ethical committee and that had been approved for public release. Release of the data was approved after the data were anonymized which included removal of relevant patient information, de-facing and cropping procedures to ensure patient privacy in the image data. Our training and validation data were released under the CC BY-NC (Attribution-NonCommercial) license. The dataset access link is on our challenge website <https://topcow23.grand-challenge.org/data/>.

Table 1 shows the statistical summary of the image voxel information of the training and test data. For CTA, the voxel size was around 0.45 mm in the X-Y dimension, and around 0.7 mm in the Z dimension. For MRA, the voxel size was around 0.3 mm in the X-Y dimension, and around 0.6 mm in the Z dimension. MRA had in general smaller pixel spacing and slice thickness than CTA. The voxel dimension was similar between training and test data.

For the whole image size, CTA’s Z-dimension (the inferior-superior dimension) was longer than MRA Z-dimension because despite the brain-mask cropping, CTA usually had the whole head scanned while our MRA data tended to leave out the region near the top of the skull. So CTA typically had larger field of view than the MRA especially near the superior region of the brain.

Table 1 also shows the dimensions of the CoW ROI, which was part of our provided annotations. The CoW ROI size was consistent between MRA and CTA modalities. But the test set had slightly larger ROI size especially along the X-dimension (left-right dimension), 45 mm in X-dimension in training versus 49 mm in test set. This was because the testset was annotated later than the training set, and there was a shift towards including slightly more MCA segments along the X or left-right dimension in the ROI. The segmentation ground truth was still covering a larger volume than the CoW ROI size, so the segmentation evaluations were not affected.

2.10. Inclusion and Exclusion of CoW Variants

We tried to include as many diverse CoW variants as possible in our challenge dataset. From our observation, the following variants were **included** and annotated in our training and test dataset:

- ✓ with or without Acom (*Note: Acom determines A1/A2*)
- ✓ double Acom
- ✓ with or without Pcom (*Note: Pcom determines P1/P2*)
- ✓ the triple ACA variant or 3rd-A2
- ✓ aplastic or hypoplastic A1 or P1 segments
- ✓ fetal PCA variants
- ✓ when CoW vessels (e.g. ACA, PCA, Acom) have fenestrations

However, there are some rare variants of which the topology cannot be characterized by our CoW multiclass labels. These variants are much less common than the ones we have included, and our thirteen CoW segment labels are insufficient to describe the complex anatomy of these rare variants. Here is a list of such CoW variants that we had observed and tried to **exclude** from our dataset:

- ✗ azygos ACA or when the left and right ACAs are fused
- ✗ anterior choroidal artery (AChA) course and supply replacing an ipsilateral fetal PCA
- ✗ duplicated PCA
- ✗ persistent primitive trigeminal artery between ICA and BA

In Fig. 3, on the left, we provide a schematic diagram of the CoW that we aim to characterize topologically, and on the right, we list some common and representative CoW variants that we have included in our dataset.

2.11. CoW Variants Prevalence

Fig. 3 right side summarizes the prevalence analysis of representative CoW anterior and posterior variants. In particular, we counted the frequency of three representative anterior variants: with Acom, missing Acom, or with a 3rd-A2; and four posterior variants: whether there are both left and right Pcoms present, or only a single-side Pcom present, or no Pcoms. Majority of the patients in our dataset had the with-Acom anterior variant (around 65 – 70%). The more prevalent posterior variants were with-both-Pcoms (around 30%) and no-Pcoms (around 35%). The prevalence of variants did not differ too much between the train and test sets.

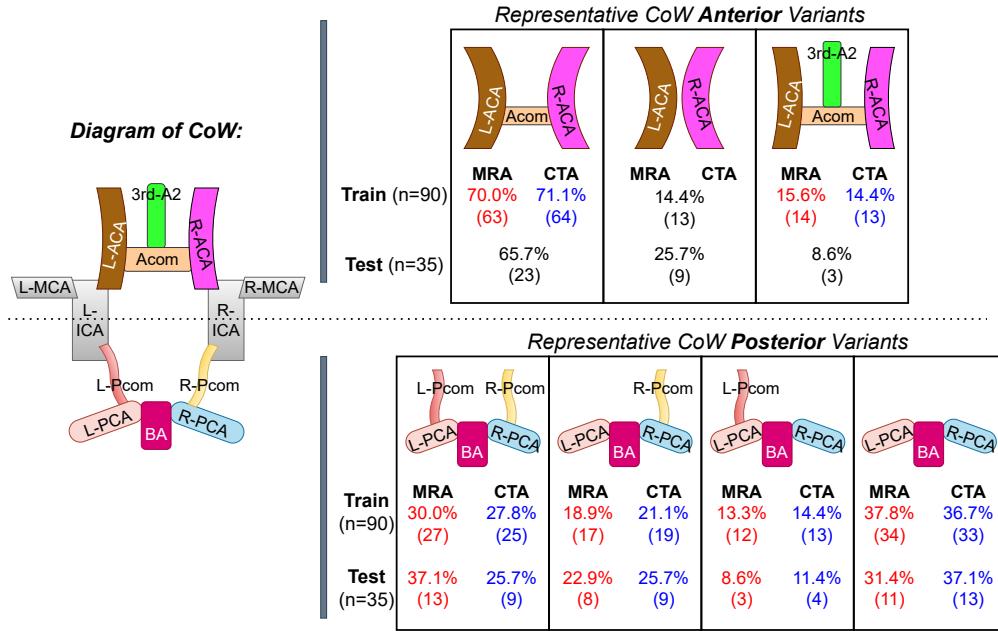


Fig. 3. Left: Schematic diagram of the CoW with all thirteen possible components. Right-top: Three representative CoW anterior variants with their frequencies in brackets as counted in our training and test data. Right-bottom: Four representative CoW posterior variants with their frequencies in brackets as counted in our training and test data. Red and blue font colors highlight inter-modality disagreement.

2.12. Inter-Rater Agreement

K.Y. and F.M. from the authors were the manual annotators for the TopCoW challenge dataset. A subset of five patients from the testset was annotated by both raters with the VR annotation workflow. These five patients were selected because they covered most if not all of CoW multiclass labels, such as having the communicating arteries or even the rare 3rd-A2. The CoW anatomical annotations from both annotators were evaluated for Dice scores shown in Fig. 4. Many of the thirteen CoW component classes had around 90% Dice scores or above, with the exceptions of R-Pcom, L-Pcom, Acom, and 3rd-A2. The R-Pcom had a lower Dice score (at around 78%) than the other classes because one of the cases had a R-Pcom with a thin segment and low contrast, which made its ground-truth annotation more sensitive to threshold and window/level adjustments.

Table 2 shows the per case performance of the inter-rater agreement. The 90% class-average Dice per case indicated good agreement in raters’ multiclass voxel annotations. The merged binary mask had around 95% Dice which showed good agreement for binary segmentation annotations. Besides the Dice similarity coefficient, We also compared the raters’ annotations in terms of centerline Dice or cDice (Shit et al., 2021) and errors in connected components using zero-th Betti number β_0 . The cDice and β_0 errors both had very good inter-rater agreement at near maximum scores as shown in Table 2.

The same evaluation metrics were used for benchmarking the submissions for the segmentation task, as we will elaborate in Section 3.4.

2.13. Inter-Modality Agreement

Fig. 3 right side shows the distribution of representative anterior and posterior CoW variants for both modalities in our training and test sets. Inter-modality disagreement are highlighted in

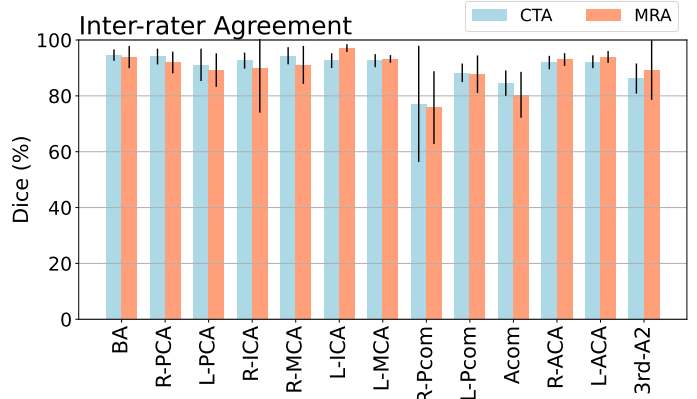


Fig. 4. Inter-rater agreement on a subset of the testset (n = 5) for all 13 CoW component classes in Dice scores ± standard deviations. Note that the n for R-Pcom, L-Pcom, and 3rd-A2 are 3, 3, 3 for CTA and 4, 4, 3 for MRA respectively.

red and blue fonts. For anterior variants, there was good inter-modality agreement especially for test set (100% agreement). The one disagreement for 3rd-A2 vs with-Acom variants came from one of the patients from training data (patient Case 008). For posterior variants, CTA disagreed with MRA especially for Pcom diagnosis, as seen in the higher count of with-both-Pcoms variants in MRA. This may be due to the proximity of the Pcoms to the sphenoid and clinoid bone regions at the skull base in CTA modality.

Qualitative comparison of inter-modality agreement can be further seen in our figures showing paired modalities of the same patients: see Fig. 2 for patient Case 083; see Fig. 8 and Fig. 9 for patients Case 114, Case 116, Case 120 and Case 126.

Table 2. Inter-rater agreement results (mean \pm standard deviation) on a subset of the testset ($n = 5$) for MRA and CTA in terms of binary and class average Dice scores, centerline Dice (cIDice) scores, binary and class average errors of the zero-th Betti number β_0 . The binary Dice, binary β_0 errors, and cIDice scores were computed on the merged binary class. The class-average Dice scores and β_0 errors were computed for each class separately and the average was taken per case. The arrow indicates the favorable direction.

Modality	Inter-rater Agreement for Challenge Metrics				
	Binary Dice (%) \uparrow	Per case class-average Dice (%) \uparrow	cIDice (%) \uparrow	Binary β_0 error \downarrow	Per case class-average β_0 error \downarrow
CTA	94.86 \pm 2.24	90.91 \pm 3.35	99.72 \pm 0.24	0 \pm 0	0 \pm 0
MRA	96.49 \pm 2.01	90.21 \pm 4.02	99.49 \pm 0.80	0.4 \pm 0.55	0.07 \pm 0.07

3. Challenge Setup and Evaluation Methods

3.1. Two Tracks and Two Tasks

Our challenge had two tracks as shown in Fig. 2, namely a CTA track and an MRA track for the same segmentation tasks. The tasks were to segment the CoW vessels (binary segmentation) and anatomical components of the CoW (multiclass segmentation). For binary segmentation task, the binary vessel label was generated by merging the annotated multiclass labels. A case for a segmentation task was the 3D angiographic imaging scan for that modality track. There were four leaderboards, one for each track-task combination. Members of the organizers’ direct research groups could participate and be included in the leaderboards. However, they were not eligible for awards. Top three teams for segmentation performance from each of the four leaderboards were publicly named as shown on the grand-challenge leaderboard webpage, and given a small Swiss wooden toy cow as a souvenir at the in-person challenge event. There were no monetary awards given.

3.2. Input and Runtime for Docker Submissions

The input to the submitted algorithm was a pair of CTA and MRA from a patient, irrespective of whether the algorithm used both modalities or not. In case the submission only needed one of the modality, it could simply ignore the other modality input.

The input to the inference algorithm was the whole image volume. But the evaluation was conducted in the CoW ROI. The CoW ROIs of the test set were not available to the participants, but were used by our evaluation to calculate the metrics.

The submitted algorithms must be fully-automatic in the form of docker containers. These docker containers were run in the cloud on the challenge platform hosted by grand-challenge.org. The cloud infrastructure provided Nvidia GPU with 16GB memory. The docker containers did not have access to internet when running the algorithm. The runtime the algorithm had for each test set case was limited to 15 minutes. Each team was given only one opportunity to upload their containers for the hidden test set to prevent overfitting on the testset.

3.3. Usage of External Training Data

Participants were allowed to use any other public datasets and private in-house data, or modify the supplied TopCoW 2023 training data, provided that they disclosed any additional or modified training datasets in their description of the submitted algorithm.

3.4. Challenge Evaluation Metrics

The segmentation results were evaluated only within the CoW ROI. We did not assess the segmentation performance on the peripheral and further downstream vessels outside the CoW ROI. Participants should focus on segmenting the CoW vessel components necessary to characterize the CoW angiography architecture.

An emphasis of this challenge was on topology-aware segmentations of CoW vessels. The assessment of algorithms followed our prior work focusing on topological properties (Shit et al., 2021; Stucki et al., 2023; Menten et al., 2023). We used Dice coefficient and centerline-Dice (cIDice) (Shit et al., 2021) for the CoW vessels, and topology-based metrics like errors of Betti numbers for connected components. The zero-th Betti number β_0 measures the number of connected components in a shape.

Three evaluation metrics with equal weights for binary (merged CoW vessel vs background) were used for segmentation task:

1. Dice similarity coefficient
2. centerline Dice (cIDice)
3. zero-th Betti number β_0 errors

Three evaluation metrics with equal weights were used for multiclass (CoW anatomical vessels) segmentation task:

1. Class-average Dice similarity coefficient
2. cIDice on merged binary mask
3. Class-average zero-th Betti number β_0 errors

The ranking for the awards of the MICCAI event was based on the leaderboards displayed on grand-challenge website. The leaderboard used equal weights for metrics column, and used the mean of several columns’ positions/ranks, or ‘rank then average’.

3.5. Beyond Segmentation Evaluations

The following *beyond segmentation* evaluations were not part of the TopCoW 2023 challenge metrics, but were done post-challenge as additional topological analysis.

3.5.1. Detection of CoW Components

The detection was computed based on the Dice scores for a CoW component: A Dice score > 0 for a CoW component was counted as a true positive (TP), regardless of the quality of the segmentation; the absence of the Dice was counted as a true negative (TN); a Dice score of 0 for a component was counted as either a false positive (FP) or a false negative (FN), depending on the presence of ground truth labels. We evaluated the detection performance in terms of recall and precision for a CoW component class.

3.5.2. CoW Variant Topology Matching

In the variant topology matching analysis, we evaluated if the predicted segmentation masks matched the topology of the representative CoW anterior and posterior variants as shown in Fig. 3.

The three anterior variant topologies evaluated were 1. with Acom; 2. missing Acom; 3. Acom with a 3rd-A2. To get a match in the topology of the **anterior** variants, the following connectivity and neighborhood conditions must be satisfied:

- Acom: correctly detected presence/absence. If present it must connect to both ACAs and have no β_0 errors
- 3rd-A2: correctly detected presence/absence. If present it must connect to the Acom and have no β_0 errors
- ACAs: have no β_0 errors and must have correct neighbourhood information (i.e. connecting to ICA if A1 is present or just connecting to Acom if A1 is missing)

The four posterior variant topologies evaluated were: 1. both R-Pcom and L-Pcom present; 2. only R-Pcom present; 3. only L-Pcom present; 4. no Pcoms. To get a match in the topology of the **posterior** variants, the following connectivity and neighborhood conditions must be satisfied:

- Pcoms: correctly detected presence/absence. If present it must connect to both ICA and PCA and have no β_0 errors
- PCAs: have no β_0 errors and must have correct neighbourhood information (i.e. connecting to BA if P1 is present or just connecting to Pcom if P1 is missing)

4. Results

4.1. Participation and Submissions

TopCoW 2023 attracted 146 registered participants from four continents. The participants formed into 27 teams, out of which 20 teams successfully made a reasonable submission to our challenge. Eventually 18 teams were qualified as co-authors and included in this challenge summary paper. Fig. 5 shows the distribution of team participating in each track-task combination. One team took part in CTA binary segmentation task only. Two teams took part in MRA binary segmentation task only. A few teams took part in a specific modality or a specific task. But taking part in all four track-task combinations was the most popular option for the participants (7 out of the 18 teams).

We summarize the methods from all the participating teams in Table 3 in alphabetical team name order. The top three teams (excluding the organizers) from the four leaderboards were awarded during the MICCAI result announcement, which are shown as colored circles in the ‘Awards’ column. For a full description of the submitted algorithms, including a baseline algorithm from the organizers, please refer to the Appendix A. Here we make some meta-observations from all submissions:

- **None required multi-modal input:** All 18 teams used single-modal input. Probably with the only exceptions from teams ‘WilliWillsWissen’ and ‘EURECOM’ trained their models taking in either CTA or MRA modality, or modality-agnostic for the single-modal input.

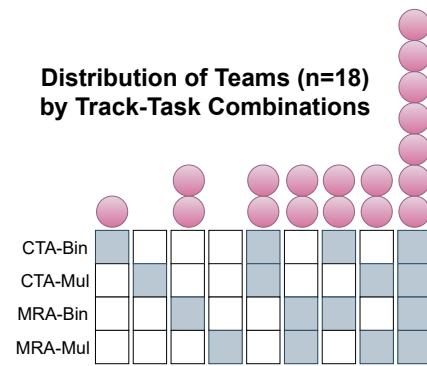


Fig. 5. Histogram of number of teams vs bins of track-task combinations. The tracks can be CTA or MRA. The tasks can be binary (Bin) or multi-class (Mul) segmentation. Each histogram bin is a vertical column of four possible participation (gray means taken part while white means no). The circles represent the number of teams for that bin.

- **Trained with both modalities?** Teams ‘WilliWillsWissen’ and ‘EURECOM’ trained their modality-agnostic model with both CTA and MRA modalities in a common pool. The ‘Organizers’ used both modalities for data augmentation.
- **None used external training data:** None of the 18 teams used additional training data.
- **Deep-learning (DL):** All the teams used DL based algorithms except for team ‘ysato’ that used a non-DL approach, which used CPU and had a short inference time (~15s).
- **2D vs 3D image:** Only two teams ‘EURECOM’ and ‘NIC-VICOROB-2’ used 2D slices in their models while the others all worked with 3D data.
- **Atlas:** Two teams ‘gl’ and ‘refrain’ employed brain atlas for registration and ROI extraction.
- **CoW ROI or custom ROI:** Around half of the teams made use of some form of ROI in their methods, which could be either the provided CoW ROI or some custom ROI obtained by atlas-registration or detection from binary mask.
- **Architecture (nnUNet or not):** There were various architectures used, but around half of the teams converged to nnUNet (Isensee *et al.*, 2021).
- **Topological optimizations:** Three teams ‘WilliWillsWissen’, ‘UB-VTL’, and ‘NexToU’ employed methods for topological objects of interest such as the skeletons and centerlines of the vessels.

Next we present the performance results from binary and multiclass segmentation tasks in the following subsections.

4.2. Binary Segmentation Performance

For binary segmentation task, thirteen teams participated in the MRA track and twelve teams participated in the CTA track. Table 4 shows the results of the binary segmentation task for MRA and CTA tracks. If participants only submitted for the

Table 3. Method summary of all participating teams, ordered alphabetically by team name. For detailed descriptions and relevant references cited, please refer to the Appendix A. Awards lists the number of first (gold), second (silver) and third (bronze) prizes a team has won in the TopCoW challenge. The winning team names are in bold.

Team	Track	Task	Awards	Method	Highlights
2i_mtl	CTA	Binary		3D AttentionUNet for segmentation; 3D autoencoder to mitigate false positives	- Use provided CoW ROI for training - Image & mask input to autoencoder
agaldran	CTA MRA	Binary Multiclass		3D dynamic UNet	- Ensembling - Cross-validation on patch size
EURECOM	CTA MRA	Binary		SynthSeg for Brain mask extraction; A2V for multi-modal segmentation	- Single model for both modalities - 2D axial slice input - Use provided CoW ROI for patch extraction
gbCoW	MRA	Binary Multiclass		3D nnUNet	- Only multiclass labels used - Turned off data augmentation
gl	CTA MRA	Multiclass		Atlas registration for custom ROI extraction; 3D MedNexT & UX-Net for binary and subsequent multiclass segmentation	- Dataset specific atlas - Binary mask input for multiclass segmentation - Ensembling
IWantToGoToCanada	CTA	Binary Multiclass		3D nnUNet for binary segmentation; 3D Swin-UNETR for subsequent multiclass segmentation	- Binary mask input for multiclass segmentation
junqiangchen	CTA MRA	Binary Multiclass		VNet3D for custom ROI extraction; VNet3D for ROI segmentation	- Brain mask extraction - Binary mask for custom ROI
IWM	CTA MRA	Binary Multiclass		3D ResidualUNet	- Custom end-to-end UNet
NexToU	CTA MRA	Binary Multiclass	● ●	3D nnUNet for low-res binary segmentation; NexToU architecture for full-res cascading	- Centerline boundary Dice (cb-Dice) - Binary topological interaction (BTI) module
NIC-VICOROB-1	CTA MRA	Binary Multiclass	● ●	3D nnUNet	- Ensembling - Binary mask input for CT multiclass
NIC-VICOROB-2	CTA MRA	Binary Multiclass		3D AttentionUNet for binary segmentation; 2D AttentionUNet for subsequent multiclass segmentation	- Axial slice input for multiclass segmentation - Binary mask input for multiclass segmentation - Use provided CoW ROI for 3D patch extraction
Organizers	CTA MRA	Multiclass	● ●	nnDetection for custom ROI extraction; 3D nnUNet for multiclass segmentation	- Image registration for data augmentation - ROI object detection - Ensembling
refrain	MRA	Binary Multiclass	●	Atlas registration for custom ROI extraction; 3D nnUNet for segmentation	- Data augmentation for rare CoW variants - Segment specific loss weighting
sjtu_eiee_2-426lab	CTA	Binary Multiclass	● ●	3D nnUNet for custom ROI extraction; 3D nnUNet for ROI segmentation	- Binary mask for custom ROI
UB-VTL	CTA MRA	Binary		Modified 3D Brave-Net	- cDice loss for connectedness - Residual connections & PReLU activations - Use provided CoW ROI for patch extraction
UW	MRA	Binary	●	3D nnUNet	- 3-component loss (Dice + CE + TopK) - Ensembling
WilliWillsWissen	CTA MRA	Binary Multiclass	● ●	3D nnUNet	- cDice/skeleton recall for connectedness - Training on both modalities - Ensembling
ysato	MRA	Binary		Auto vessel thresholding; Region growing	- Non-deep learning algorithm - Short inference time (~15s per case) - Little computing power needed (done on CPU)

multiclass segmentation, the results were automatically evaluated for binary segmentation and inserted in the table as well (two teams marked with a ‘*’).

The winning teams for the binary segmentation task were ‘WilliWillsWissen’, ‘NIC-VICOROB-1’, and ‘UW’ for the MRA track; and ‘sjtu_eiee_2-426lab’, ‘WilliWillsWissen’, and ‘NIC-VICOROB-1’ for the CTA track. Team ‘WilliWillsWissen’ and ‘NIC-VICOROB-1’ had good performance scores for both modalities. As seen from Table 4, non-winning teams also had good performance for certain individual metrics, such as teams ‘refrain’, ‘NexToU’, and ‘organizers’. The winning teams in general had above 92% Dice scores, above 97% cDice scores, and below 0.6 β_0 errors.

Although the quantitative metric scores were high and very close to the inter-rater agreement, there could still be subtle topological problems such as broken vessels especially when the vessel segments were around 1 mm in diameter or thinner, and when the thin segments were elongated in length, as illustrated in Fig. 6. The predicted binary segmentation for Case 114 had a fragmented segment and a small floating blob on the right. The predicted binary segmentation for Case 120 had a broken segment on the left. The binary segmentation results were close to the ground truth despite some subtle topological errors.

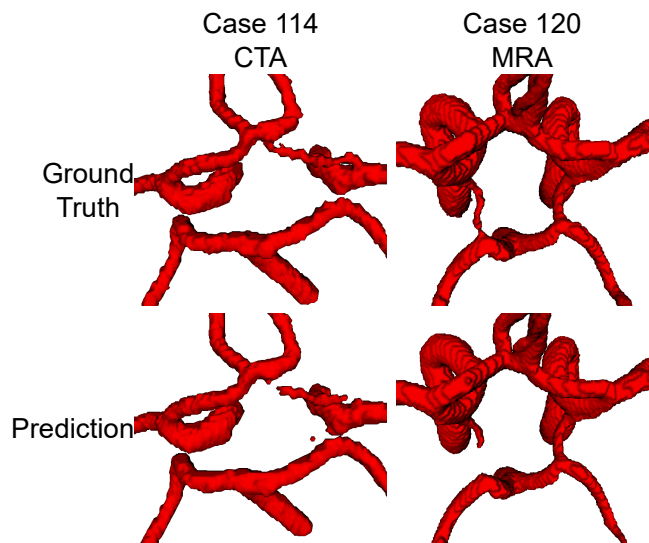


Fig. 6. Qualitative results of binary segmentation task with subtle topological mistakes despite the high performance on the metrics. The predictions are by team ‘WilliWillsWissen’ compared with ground truth binary mask.

Table 4. Binary segmentation task results (mean \pm standard deviation) for MRA and CTA in Dice scores, centerline Dice (cDice) scores and errors in the zero-th Betti number β_0 . The arrow indicates the favorable direction. The top three values for each metric and each track are marked as gold, silver and bronze cells in decreasing order. A ‘*’ behind the team name means that the segmentation predictions have been converted from the multiclass submissions and inserted here. If a team only submitted to one of the tracks the columns of the other track are filled with a ‘-’. The winning team names are in bold.

Team	Binary segmentation performance					
	MRA			CTA		
	Dice (%) \uparrow	cDice (%) \uparrow	β_0 error \downarrow	Dice (%) \uparrow	cDice (%) \uparrow	β_0 error \downarrow
2i_mtl	-	-	-	44.15 \pm 11.94	48.04 \pm 11.23	28.77 \pm 15.12
agaldran	94.33 \pm 2.64	96.68 \pm 2.79	1.57 \pm 1.29	87.73 \pm 3.26	95.99 \pm 2.97	2.26 \pm 1.82
EURECOM	93.84 \pm 2.69	94.42 \pm 3.10	3.77 \pm 2.79	84.79 \pm 4.34	89.92 \pm 5.43	8.14 \pm 4.66
gbCoW	94.95 \pm 2.89	98.10 \pm 2.33	0.86 \pm 0.94	-	-	-
gl*	93.67 \pm 4.84	95.81 \pm 5.11	0.71 \pm 0.86	70.94 \pm 24.88	75.80 \pm 28.05	2.09 \pm 1.48
IWantToGoToCanada	-	-	-	90.06 \pm 2.67	96.56 \pm 2.65	1.40 \pm 0.88
junqiangchen	94.09 \pm 2.08	96.86 \pm 2.80	3.20 \pm 2.96	89.49 \pm 2.87	95.91 \pm 1.63	3.91 \pm 2.84
IWM	94.39 \pm 2.48	97.39 \pm 2.76	1.43 \pm 1.36	91.07 \pm 2.50	97.07 \pm 2.60	1.74 \pm 1.27
NexToU	94.05 \pm 2.91	97.29 \pm 2.29	0.69 \pm 0.68	92.28 \pm 2.83	97.70 \pm 2.54	0.77 \pm 0.97
NIC-VICOROB-1	95.60 \pm 2.32	98.26 \pm 2.20	0.60 \pm 0.60	92.07 \pm 3.54	97.93 \pm 2.47	0.60 \pm 0.85
NIC-VICOROB-2	93.13 \pm 3.67	94.30 \pm 7.03	17.69 \pm 57.63	89.68 \pm 3.87	95.45 \pm 3.28	3.80 \pm 2.74
Organizers*	95.14 \pm 2.90	98.06 \pm 2.30	0.57 \pm 0.65	90.25 \pm 5.73	96.98 \pm 3.48	1.14 \pm 1.44
refrain	93.87 \pm 2.02	98.20 \pm 1.84	0.97 \pm 1.20	-	-	-
sjtu_eiee_2-426lab	-	-	-	92.75 \pm 3.19	97.81 \pm 2.66	0.40 \pm 0.55
UB-VTL	91.78 \pm 2.41	93.27 \pm 3.50	0.91 \pm 0.98	72.27 \pm 6.89	77.49 \pm 7.92	2.37 \pm 1.72
UW	95.37 \pm 2.20	98.18 \pm 1.93	0.89 \pm 0.87	-	-	-
WilliWillsWissen	95.54 \pm 2.72	98.31 \pm 2.14	0.37 \pm 0.60	92.16 \pm 2.76	98.42 \pm 1.83	0.57 \pm 0.81
ysato	88.05 \pm 4.94	91.99 \pm 3.60	2.60 \pm 1.77	-	-	-

4.3. Multiclass Segmentation Performance

Thirteen teams took part in the multiclass segmentation task, of which nine teams took part for both the MRA track and the CTA track. The winning teams for the CTA track were ‘WilliWillsWissen’, ‘NexToU’, ‘organizers’, and ‘sjtu_eiee_2-426lab’. For the MRA track, the winning teams were ‘WilliWillsWissen’, ‘organizers’, ‘refrain’, and ‘NexToU’.

Table 5 shows the Dice scores and β_0 errors for each individual CoW component class. Some non-winning teams performed well for certain individual CoW components. Such as teams ‘gl’ and ‘NIC-VICOROB-1’, they had low β_0 errors for MRA track. Team ‘IWM’ had low β_0 errors for a few CoW components for CTA track. Team ‘IWantToGoToCanada’ had good Dice scores for a few CoW components, although the β_0 errors were high. Team ‘NIC-VICOROB-1’ also had very good performance on 3rd-A2 for CTA track and Acom for MRA track. Non-winning team ‘gbCoW’ could segment the 3rd-A2 class well for MRA track. The winning teams in general achieved top-3 values in Dice scores and β_0 errors across all CoW components.

However, even judging from the top-3 values for each CoW class, there was a big gap between two groups of CoW anatomical components:

- ✓ **Group 1: Non-communicating arteries that are almost always present (BA, PCA, ICA, MCA, ACA).** These structures were well segmented at 85 – 95% Dice scores while having β_0 errors of around 0 to 0.09.
- ✗ **Group 2: Communicating arteries (Acom, Pcom) and the rare 3rd-A2.** They are often thinner and smaller structures, and can be missing in CoW. These Group 2 structures had lower and more varying Dice scores between 52 – 68%. The β_0 errors were also higher, such as at least 0.37 for R-Pcom and 0.53 for L-Pcom in CTA modality.

Fig. 7 shows the average Dice scores of Group 1 and Group 2 CoW components from the top performing teams for each track. It can be seen that Group 1 components were segmented at around 85% Dice while Group 2 components were only segmented at around 50% by the top teams.

To investigate the above-mentioned performance gap between the two groups of CoW anatomical components that existed even for the top submissions, we selected four patients from the test set with as a wide range of CoW variants to compare the segmentation results qualitatively. The four patients were Case 114, Case 116, Case 120 and Case 126. Both the CTA (Fig. 8) and MRA (Fig. 9) modalities are shown. Predictions from the winning teams are listed along with the ground truth mask. We highlight a few key observations from the qualitative results for each case and for both modalities in the following list:

- **Case 114 (Hypoplastic R-A1, No Pcoms):** This patient’s R-ACA has a thicker A2 and thinner (hypoplastic) A1 segment with around 1 mm in diameter. This hypoplastic R-A1 morphology turned out to be difficult as many teams wrongly segmented the R-A1 broken half-way or without touching the R-ACA. Team ‘WilliWillsWissen’ had slightly better connectivity for R-A1. Some teams also falsely detected the presence of R-Pcom and wrongly segmented some fragments near the R-ICA as R-Pcom. For CTA modality, team ‘sjtu_eiee_2-426lab’ mirror-flipped the left and right labels wrongly.
- **Case 116 (No Acom, only R-Pcom):** Human raters often struggled with deciding if there is Acom when ACA tubular surfaces touch sideways like in this patient. The ACAs touch but the ground truth annotation was verified to be without Acom despite that touching region. All teams wrongly detected the presence of Acom at the touch site. The single R-Pcom was correctly segmented by most teams, except for CTA’s team ‘sjtu_eiee_2-426lab’ that flipped the left and right sides.
- **Case 120 (3rd-A2, both Pcoms):** This patient has a 3rd-A2 but is not easily diagnosed, as the 3rd-A2 is thin with around 1 mm in diameter and is tangled with the R-A2. Teams ‘refrain’ and ‘NexToU’ managed to detect the presence of the 3rd-A2 for the MRA modality, but their predicted 3rd-A2 segments were not connected to Acom, resulting in topological errors. The L-Pcom is thin with

Table 5. Multiclass segmentation task results of all 13 CoW component classes (mean \pm standard deviation) for the CTA (Top) and MRA (Bottom) tracks in Dice scores and β_0 errors. The arrow indicates the favorable direction. The top three values for each metric are marked as gold, silver and bronze cells in decreasing order. The winning team names are in bold.

Team	CTA per class segmentation performance												
	BA	R-PCA	L-PCA	R-ICA	R-MCA	L-ICA	L-MCA	R-Pcom	L-Pcom	Acom	R-ACA	L-ACA	3rd-A2
	Dice (%) \uparrow												
agaldran	1.33 \pm 6.02	0.00 \pm 0.00	0.02 \pm 0.09	0.00 \pm 0.00	0.00 \pm 0.00	0.00 \pm 0.00	0.00 \pm 0.00	0.00 \pm 0.00	0.00 \pm 0.00	0.00 \pm 0.00	0.00 \pm 0.00	0.00 \pm 0.00	0.00 \pm 0.00
gl	75.48 \pm 24.75	59.25 \pm 29.61	58.99 \pm 34.52	70.88 \pm 28.46	65.83 \pm 31.94	71.84 \pm 26.06	63.52 \pm 31.93	11.33 \pm 20.97	10.28 \pm 21.75	0.00 \pm 0.00	59.89 \pm 29.90	55.55 \pm 35.09	0.00 \pm 0.00
IWantToGoToCanada	90.47 \pm 5.28	85.70 \pm 7.46	86.83 \pm 5.56	87.80 \pm 7.44	84.78 \pm 13.84	89.49 \pm 5.33	85.79 \pm 8.39	42.10 \pm 34.98	31.23 \pm 37.51	46.14 \pm 34.01	81.63 \pm 11.93	83.55 \pm 10.68	9.62 \pm 24.74
junqiangchen	91.37 \pm 3.77	85.32 \pm 7.54	85.78 \pm 7.58	87.17 \pm 4.75	86.57 \pm 7.49	86.01 \pm 15.42	84.73 \pm 7.50	34.42 \pm 34.21	26.81 \pm 36.16	42.47 \pm 33.34	80.79 \pm 13.01	82.03 \pm 12.19	4.05 \pm 15.34
IWM	86.25 \pm 16.57	86.71 \pm 6.52	83.32 \pm 14.25	87.41 \pm 6.18	87.20 \pm 7.63	87.53 \pm 6.67	85.01 \pm 9.82	0.00 \pm 0.00	0.00 \pm 0.00	0.00 \pm 0.00	82.17 \pm 12.16	84.84 \pm 9.73	0.00 \pm 0.00
NexToU	90.00 \pm 6.34	86.91 \pm 6.63	88.34 \pm 5.36	89.21 \pm 4.65	87.80 \pm 6.68	89.36 \pm 4.41	85.84 \pm 7.46	61.68 \pm 26.86	42.68 \pm 36.62	59.49 \pm 29.33	84.67 \pm 9.12	86.22 \pm 9.25	0.00 \pm 0.00
NIC-VICOROB-1	92.15 \pm 3.89	52.17 \pm 41.78	51.09 \pm 40.27	52.48 \pm 41.72	49.51 \pm 38.49	46.72 \pm 42.92	36.22 \pm 40.34	31.78 \pm 37.15	27.92 \pm 36.65	50.79 \pm 34.54	49.74 \pm 40.65	50.09 \pm 39.20	52.70 \pm 45.65
NIC-VICOROB-2	83.54 \pm 11.97	76.93 \pm 12.82	72.57 \pm 15.52	81.02 \pm 9.52	78.34 \pm 12.07	81.00 \pm 11.15	73.30 \pm 12.22	27.57 \pm 27.74	12.00 \pm 18.36	11.73 \pm 18.70	67.89 \pm 17.16	71.47 \pm 12.91	0.63 \pm 1.56
Organizers	93.37 \pm 3.02	84.40 \pm 21.61	82.69 \pm 22.28	86.40 \pm 16.14	82.83 \pm 20.02	88.12 \pm 11.70	81.47 \pm 22.13	43.27 \pm 37.54	32.21 \pm 33.62	57.36 \pm 30.57	80.72 \pm 16.59	84.06 \pm 12.00	43.15 \pm 42.25
sjtu_eiee_2-426lab	93.12 \pm 2.98	72.93 \pm 34.68	70.48 \pm 36.17	70.75 \pm 36.46	68.92 \pm 36.24	69.56 \pm 36.41	65.29 \pm 39.76	46.18 \pm 35.55	38.62 \pm 39.07	54.86 \pm 35.92	66.76 \pm 35.46	67.54 \pm 35.65	33.93 \pm 42.17
WilliWillsWissen	91.29 \pm 6.55	89.59 \pm 5.07	89.56 \pm 5.72	89.74 \pm 4.61	89.05 \pm 7.09	90.57 \pm 3.75	87.32 \pm 7.69	57.49 \pm 31.84	52.00 \pm 34.48	56.65 \pm 31.73	88.04 \pm 6.21	88.73 \pm 5.60	39.19 \pm 36.73
β_0 error \downarrow													
agaldran	0.71 \pm 0.52	1.49 \pm 1.31	1.71 \pm 2.11	0.94 \pm 0.34	0.94 \pm 0.24	1.03 \pm 0.17	0.89 \pm 0.40	0.94 \pm 0.24	1.00 \pm 0.00	1.00 \pm 0.00	1.17 \pm 0.66	0.94 \pm 0.54	1.00 \pm 0.00
gl	0.06 \pm 0.24	0.09 \pm 0.28	0.09 \pm 0.28	0.11 \pm 0.32	0.14 \pm 0.36	0.14 \pm 0.55	0.20 \pm 0.41	0.71 \pm 0.55	0.79 \pm 0.42	1.00 \pm 0.00	0.11 \pm 0.32	0.06 \pm 0.24	1.00 \pm 0.00
IWantToGoToCanada	0.31 \pm 0.76	0.74 \pm 1.24	0.80 \pm 1.08	0.40 \pm 1.01	0.11 \pm 0.40	0.60 \pm 1.17	0.23 \pm 0.49	1.41 \pm 1.37	1.36 \pm 1.11	0.50 \pm 0.79	1.66 \pm 1.57	1.06 \pm 1.45	1.80 \pm 1.26
junqiangchen	0.06 \pm 0.24	0.43 \pm 0.74	0.80 \pm 1.02	0.06 \pm 0.24	0.20 \pm 0.47	0.14 \pm 0.36	0.26 \pm 0.61	1.62 \pm 1.58	2.12 \pm 1.37	0.37 \pm 0.60	1.56 \pm 0.70	0.66 \pm 1.00	6.97 \pm 3.30
IWM	0.03 \pm 0.17	0.43 \pm 0.66	0.26 \pm 0.66	0.03 \pm 0.17	0.06 \pm 0.24	0.03 \pm 0.17	0.06 \pm 0.24	1.00 \pm 0.00	1.00 \pm 0.00	1.00 \pm 0.00	0.57 \pm 0.78	0.31 \pm 0.68	1.00 \pm 0.00
NexToU	0.03 \pm 0.17	0.17 \pm 0.38	0.14 \pm 0.49	0.09 \pm 0.37	0.03 \pm 0.17	0.06 \pm 0.24	0.14 \pm 0.36	0.37 \pm 0.83	0.53 \pm 0.70	0.14 \pm 0.36	0.20 \pm 0.47	0.23 \pm 0.55	1.00 \pm 0.00
NIC-VICOROB-1	0.09 \pm 0.28	0.23 \pm 0.43	0.46 \pm 0.95	0.34 \pm 0.54	0.34 \pm 0.48	0.17 \pm 0.45	0.34 \pm 0.48	1.14 \pm 1.46	0.78 \pm 0.81	0.19 \pm 0.40	0.94 \pm 1.61	0.66 \pm 0.87	0.33 \pm 0.58
NIC-VICOROB-2	2.80 \pm 2.49	2.20 \pm 2.10	3.34 \pm 2.81	2.63 \pm 2.34	1.23 \pm 1.65	1.46 \pm 1.79	1.63 \pm 2.22	2.32 \pm 1.54	1.88 \pm 1.58	1.32 \pm 1.04	3.91 \pm 3.23	3.23 \pm 2.47	0.67 \pm 0.52
Organizers	0.00 \pm 0.00	0.09 \pm 0.37	0.20 \pm 0.53	0.00 \pm 0.00	0.03 \pm 0.17	0.00 \pm 0.00	0.06 \pm 0.24	0.93 \pm 0.92	1.04 \pm 0.88	0.19 \pm 0.40	0.40 \pm 0.95	0.37 \pm 0.84	0.33 \pm 0.58
sjtu_eiee_2-426lab	0.00 \pm 0.00	0.31 \pm 0.63	0.26 \pm 0.74	0.06 \pm 0.34	0.09 \pm 0.37	0.14 \pm 0.43	0.17 \pm 0.45	0.45 \pm 0.60	0.56 \pm 0.86	0.23 \pm 0.50	0.49 \pm 1.07	0.31 \pm 0.63	0.50 \pm 0.58
WilliWillsWissen	0.00 \pm 0.00	0.03 \pm 0.17	0.03 \pm 0.17	0.00 \pm 0.00	0.06 \pm 0.24	0.00 \pm 0.00	0.03 \pm 0.17	0.48 \pm 0.81	0.56 \pm 0.89	0.23 \pm 0.43	0.09 \pm 0.37	0.20 \pm 0.47	0.33 \pm 0.58

Team	MRA per class segmentation performance												
	BA	R-PCA	L-PCA	R-ICA	R-MCA	L-ICA	L-MCA	R-Pcom	L-Pcom	Acom	R-ACA	L-ACA	3rd-A2
	Dice (%) \uparrow												
agaldran	0.12 \pm 0.71	0.00 \pm 0.00	0.00 \pm 0.00	0.00 \pm 0.00	0.00 \pm 0.00	0.00 \pm 0.00	0.00 \pm 0.00	0.00 \pm 0.00	0.00 \pm 0.00	0.00 \pm 0.00	0.00 \pm 0.00	0.01 \pm 0.08	0.00 \pm 0.00
gbCoW	93.47 \pm 3.33	83.52 \pm 16.12	80.25 \pm 24.23	90.03 \pm 17.82	84.43 \pm 14.95	90.11 \pm 22.69	84.38 \pm 22.02	64.54 \pm 31.21	53.67 \pm 39.72	56.48 \pm 33.34	82.16 \pm 24.18	85.50 \pm 18.15	49.88 \pm 36.82
gl	90.10 \pm 15.96	87.21 \pm 11.44	86.93 \pm 12.86	92.47 \pm 11.32	88.93 \pm 6.92	94.15 \pm 7.27	89.17 \pm 6.02	45.83 \pm 38.72	49.41 \pm 39.38	51.77 \pm 35.94	81.23 \pm 22.66	87.10 \pm 9.42	24.57 \pm 39.36
junqiangchen	87.81 \pm 16.05	83.89 \pm 17.97	82.44 \pm 20.90	93.06 \pm 5.68	85.03 \pm 10.57	94.27 \pm 4.27	88.56 \pm 6.27	50.17 \pm 34.35	35.85 \pm 38.24	44.76 \pm 33.36	82.55 \pm 18.29	85.13 \pm 14.50	5.73 \pm 19.50
IWM	90.11 \pm 7.97	87.01 \pm 8.20	83.59 \pm 20.23	93.28 \pm 8.47	87.92 \pm 9.00	94.87 \pm 3.17	88.11 \pm 6.21	58.98 \pm 31.39	0.00 \pm 0.00	42.80 \pm 35.83	82.22 \pm 17.69	86.28 \pm 11.75	0.00 \pm 0.00
NexToU	90.56 \pm 6.71	89.04 \pm 7.20	88.89 \pm 11.50	92.92 \pm 8.82	88.39 \pm 9.26	94.83 \pm 3.55	89.20 \pm 6.28	66.42 \pm 25.83	64.61 \pm 32.00	48.51 \pm 34.71	84.55 \pm 18.12	88.93 \pm 7.83	54.63 \pm 25.45
NIC-VICOROB-1	93.17 \pm 3.91	83.50 \pm 23.65	80.57 \pm 27.07	85.96 \pm 26.77	77.17 \pm 29.78	86.18 \pm 28.27	79.78 \pm 29.52	60.22 \pm 33.74	47.92 \pm 40.23	58.20 \pm 31.40	75.77 \pm 32.97	80.05 \pm 29.98	20.40 \pm 40.79
NIC-VICOROB-2	86.21 \pm 6.96	80.52 \pm 13.29	79.20 \pm 12.87	90.36 \pm 9.90	76.57 \pm 16.03	91.78 \pm 5.12	79.77 \pm 11.87	25.03 \pm 28.08	26.05 \pm 33.29	19.36 \pm 22.34	72.30 \pm 18.87	74.66 \pm 14.75	3.41 \pm 13.20
Organizers	93.61 \pm 3.21	90.77 \pm 7.00	89.08 \pm 10.57	94.18 \pm 9.43	88.75 \pm 7.59	95.88 \pm 2.09	90.35 \pm 4.98	67.98 \pm 25.66	50.17 \pm 38.18	54.99 \pm 33.33	85.39 \pm 18.43	88.97 \pm 9.07	25.98 \pm 40.07
refrain	93.15 \pm 3.21	88.93 \pm 5.30	88.51 \pm 8.06	93.59 \pm 5.96	86.95 \pm 8.78	94.94 \pm 1.72	88.23 \pm 4.47	61.61 \pm 30.65	64.39 \pm 27.74	52.96 \pm 31.02	83.76 \pm 16.49	87.61 \pm 6.73	38.68 \pm 30.16
WilliWillsWissen	92.97 \pm 3.99	89.04 \pm 9.95	89.95 \pm 7.88	93.64 \pm 8.83	85.89 \pm 12.19	95.79 \pm 2.01	88.51 \pm 7.51	67.12 \pm 26.91	68.32 \pm 29.27	54.39 \pm 32.73	84.76 \pm 22.19	90.60 \pm 5.77	0.00 \pm 0.00
β_0 error \downarrow													
agaldran	0.91 \pm 0.28	1.26 \pm 1.50	1.20 \pm 1.08	1.06 \pm 0.24	1.03 \pm 0.17	1.06 \pm 0.24	1.03 \pm 0.17	0.91 \pm 0.43	1.00 \pm 0.00	1.00 \pm 0.00	0.74 \pm 0.44	0.94 \pm 0.59	1.00 \pm 0.00
gbCoW	0.00 \pm 0.00	0.46 \pm 0.61	0.40 \pm 0.81	0.14 \pm 0.55	0.14 \pm 0.43	0.17 \pm 0.45	0.20 \pm 0.41	0.38 \pm 0.77	0.55 \pm 0.60	0.34 \pm 0.65	0.37 \pm 0.81	0.40 \pm 0.74	0.25 \pm 0.50
gl	0.03 \pm 0.17	0.03 \pm 0.17	0.00 \pm 0.00	0.06 \pm 0.24	0.00 \pm 0.00	0.03 \pm 0.17	0.06 \pm 0.24	0.35 \pm 0.49	0.28 \pm 0.46	0.30 \pm 0.47	0.06 \pm 0.34	0.09 \pm 0.28	0.67 \pm 0.52
junqiangchen	0.06 \pm 0.24	0.20											

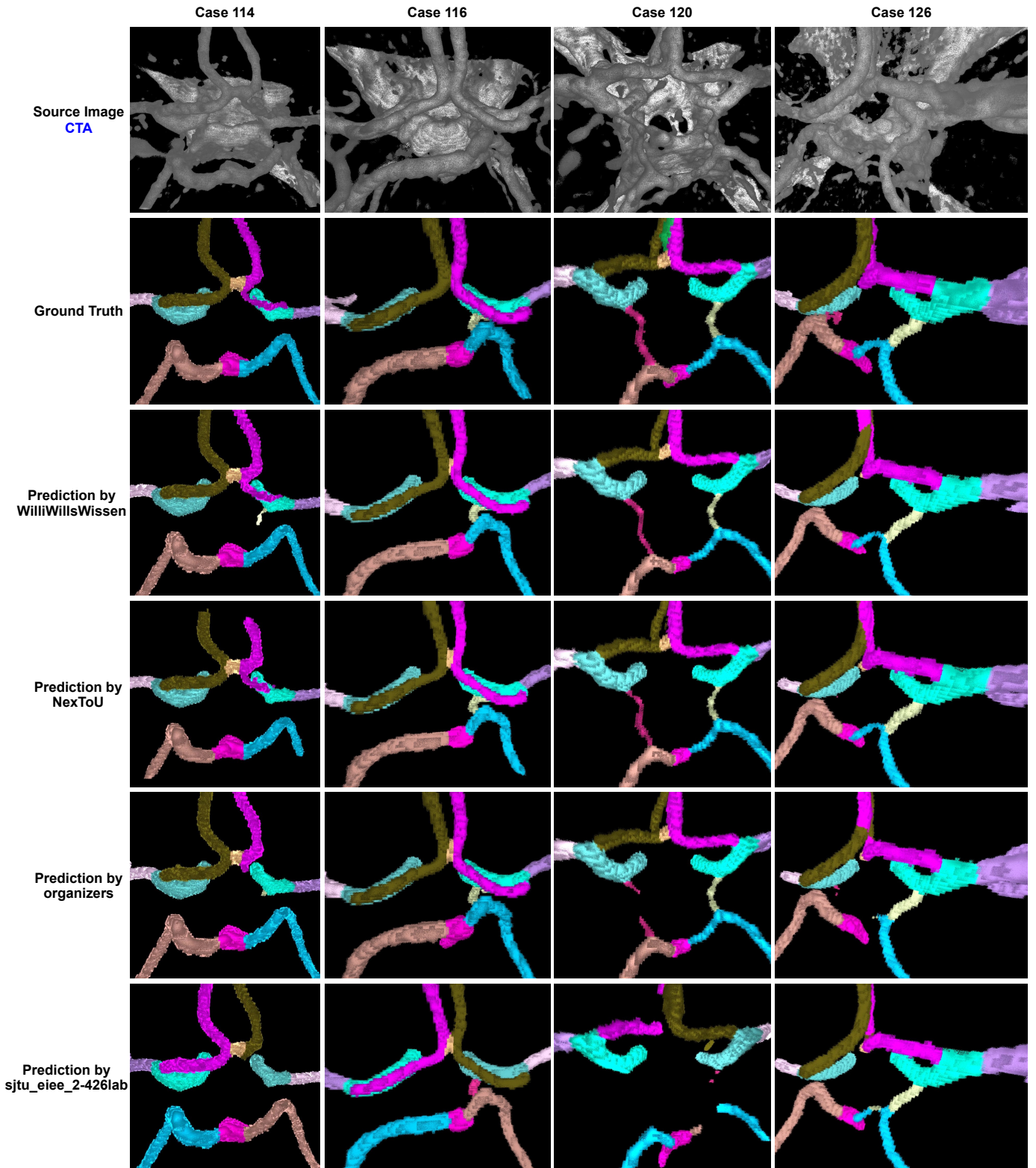


Fig. 8. Qualitative results for CTA multiclass segmentation task. The ground truth is compared with the winning teams on four selected patients from the test set. Note the same four patients are selected for both qualitative comparison figures for CTA (Fig. 8) and MRA (Fig. 9).

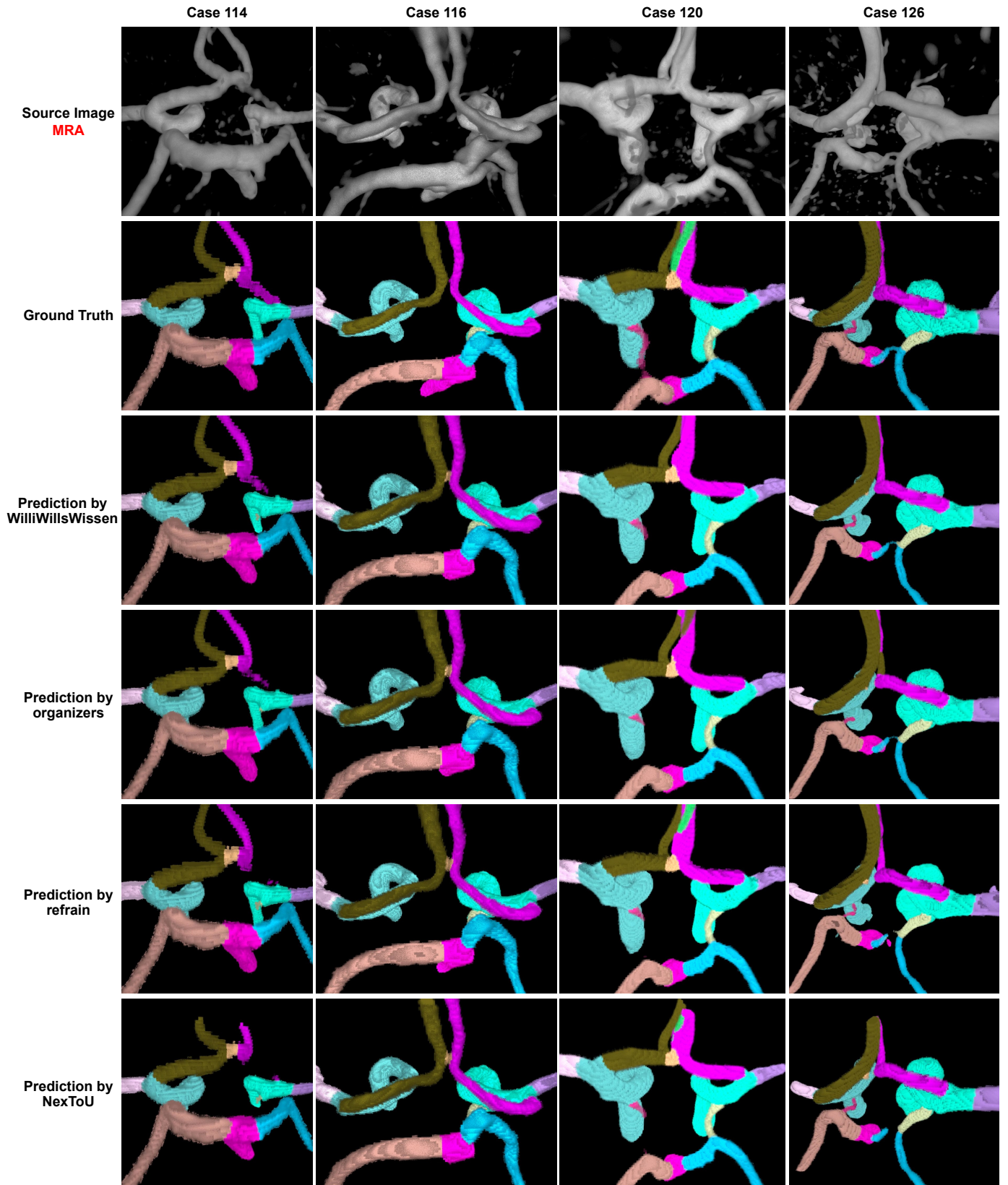


Fig. 9. Qualitative results for MRA multiclass segmentation task. The ground truth is compared with the winning teams on four selected patients from the test set. Note the same four patients are selected for both qualitative comparison figures for CTA (Fig. 8) and MRA (Fig. 9).

for CTA modality and on the L-ACA for MRA modality. The predicted ACAs could also be wrong topologically with crossover between L-ACA and R-ACA, such as in the prediction by team ‘organizers’. This patient has a fetal R-PCA, meaning the R-Pcom is thicker than the R-P1 segment of the of R-PCA. Some teams predicted the fetal R-PCA topology wrongly, such as with broken PCA in team ‘refrain’ or with PCA-Pcom crossover like in team ‘sjtu_eiee_2-426lab’. Teams ‘WilliWillsWissen’ and ‘Nex-ToU’ correctly segmented the fetal R-PCA both morphologically and topologically for the CTA modality.

As demonstrated by the qualitative results in CTA (Fig. 8) and MRA (Fig. 9), the CoW anatomical characterization problem has the potential to be solved as a multiclass segmentation task. But how well can the predicted segmentation masks actually characterize the CoW, especially its topology? To get insight on that question, we conducted two additional topological evaluations that were *beyond segmentation*. One was on the detection of certain CoW segments, and the other was on topology matching for certain CoW variants. We show the results of the beyond segmentation analysis in the next two subsections.

4.4. Beyond Segmentation Part-I: Detection of Group 2 CoW Components

To capture the underlying topology of the CoW, it is important to correctly detect the presence and absence of vessel segments. False positive (FP) and false negative (FN) in detection affect the CoW variant characterization. For example in Fig. 8 and Fig. 9, we have seen FP detection of Acom in Case 116 and Case 120, FP detection of R-Pcom in Case 114. FN detection of 3rd-A2 in Case 120, and FN detection of L-Pcom in Case 126.

The detection seemed especially challenging for the Group 2 CoW components, i.e., the communicating arteries (Acom, R-Pcom and L-Pcom) and the rare 3rd-A2 segment. Thus we evaluated the detection performance in terms of precision and recall for the aforementioned four segments for both MRA and CTA in Table 6.

The winning teams had fairly good detection performance for R-Pcom, L-Pcom, and Acom, often with 80%–90% or above for both precision and recall. Recall, which is the same as sensitivity, measures what proportion of a CoW component class is correctly detected. As we have seen from the qualitative results, many top teams were sensitive to predict the presence of Acom even with FP. This was indeed reflected in the higher recall than precision for most teams for Acom. Many teams also had a higher recall than precision for both Pcoms, indicating more FP than FN for Pcom classes. The 3rd-A2 component had less consistent detection results but the sample size ($n=3$) was also small. For example, team ‘WilliWillsWissen’ had 100% precision i.e. no FP for 3rd-A2 in CTA modality, but failed to detect any 3rd-A2 for MRA modality. Teams ‘NexToU’ and ‘refrain’ had no FP and no FN, achieving 100% precision and recall for 3rd-A2 in the MRA modality.

Detection is important in evaluating the segmentation topologically. But it is not sufficient to just look at the detection metrics for the CoW characterization problem, as we have seen

the topological mistakes with even correct detection of CoW components. For example, for Case 120 MRA modality predictions in Fig. 9, the 3rd-A2 class was correctly detected by teams ‘refrain’ and ‘NexToU’. However, the predicted 3rd-A2 was not connected to the Acom thus the topology was not correct. Other examples include the crossover mistakes in Case 126, and other broken or fragmented segments like in Case 120.

4.5. Beyond Segmentation Part-II: CoW Variant Topology Matching

One of the key applications of our multiclass segmentation task is to characterize representative CoW anterior and posterior variants. Ideally the predicted segmentation should capture the topology of the CoW variant. Therefore not only do the CoW components need to be correctly detected for their presence/absence, the topology extracted from the multiclass segmentation should also match that of the CoW variant.

As qualitative examples, we show if the predicted segmentation from one of the winning teams, ‘WilliWillsWissen’, could correctly match the topology of the ground truth for a few selected CoW anterior (Fig. 10 top) and posterior (Fig. 10 bottom) variants. We describe the CoW variants shown and whether the topologies match:

- ✓ **Case 110 with Acom:** This case has a clear Acom. The segmentations from team ‘WilliWillsWissen’ correctly matched this anterior variant topologically.
- ✗ **Case 095 with Aplastic R-A1:** This case has a missing (aplastic) R-A1 segment, and the R-A2 is supplied by the L-ACA via Acom. The prediction made a mistake segmenting part of the nearby vein wrongly as a fragment of R-ACA, resulting in a failed topology match.
- ✗ **Case 118 with No Acom:** This case has no Acom. Even though the prediction managed to predict correctly the absence of Acom, there was cross-over mistake in the L-ACA and R-ACA, resulting in a failed topology match.
- ✓ **Case 130 with 3rd-A2:** This case has a 3rd-A2 and the prediction matched the topology of this variant correctly.
- ✗ **Case 126 with Fetal R-PCA:** This case has a fetal PCA on the right side, meaning the R-Pcom is the more dominant vessel than the R-P1 segment. However, the prediction broke the R-PCA into two fragments at the contact point with R-Pcom, resulting in a failed topology match.
- ✗ **Case 115 with Fetal L-PCA:** This case has a fetal PCA on the left side. A fragment of L-PCA was wrongly segmented touching the BA, resulting in a failed topology match.
- ✓ **Case 118 with Single R-Pcom:** This case has a single Pcom on the right. The prediction correctly matched the topology of the variant.
- ✓ **Case 127 with No Pcom:** This case has no Pcoms, and the predictions correctly matched the topology of this variant.

To quantify the topology matching performance, we computed what proportion of a CoW variant was matched correctly by top teams in Fig. 11. To get a match in the topology of

Table 6. Detection performance in terms of precision and recall for the R-Pcom, L-Pcom, Acom and 3rd-A2 (i.e. Group 2 CoW components) for CTA (Top) and MRA (Bottom) tracks. Each case with a Dice score of 0 for the corresponding segment was counted as a false positive or a false negative respectively, depending on the ground truth labels. Hereby a positive refers to a segment that is present, a negative to a segment that is absent. The top three values for each metric from each track are marked as gold, silver and bronze cells in decreasing order. A ‘nan’ indicates that the corresponding value could not be computed due to division by zero. The winning team names are in bold.

CTA Precision & Recall of Group 2 CoW Components								
Team	R-Pcom (n=18)		L-Pcom (n=13)		Acom (n=26)		3rd-A2 (n=3)	
	Precision (%)	Recall (%)	Precision (%)	Recall (%)	Precision (%)	Recall (%)	Precision (%)	Recall (%)
agaldran	nan	0.0	nan	0.0	nan	0.0	nan	0.0
gl	53.8	38.9	40.0	30.8	0.0	0.0	nan	0.0
IWantToGoToCanada	65.4	94.4	52.0	100.0	75.8	96.2	20.0	100.0
junqiangchen	52.9	100.0	38.2	100.0	74.3	100.0	8.6	100.0
IWM	nan	0.0	nan	0.0	nan	0.0	nan	0.0
NexToU	94.7	100.0	68.4	100.0	92.3	92.3	nan	0.0
NIC-VICOROB-1	73.3	61.1	61.5	61.5	83.3	96.2	100.0	66.7
NIC-VICOROB-2	58.1	100.0	48.0	92.3	66.7	61.5	25.0	33.3
Organizers	66.7	100.0	56.5	100.0	83.9	100.0	100.0	66.7
sjtu.eiee.2-426lab	78.9	83.3	68.8	84.6	85.7	92.3	66.7	66.7
WilliWillsWissen	85.7	100.0	80.0	92.3	85.7	92.3	100.0	66.7

MRA Precision & Recall of Group 2 CoW Components								
Team	R-Pcom (n=21)		L-Pcom (n=16)		Acom (n=26)		3rd-A2 (n=3)	
	Precision (%)	Recall (%)	Precision (%)	Recall (%)	Precision (%)	Recall (%)	Precision (%)	Recall (%)
agaldran	0.0	0.0	nan	0.0	nan	0.0	nan	0.0
gbCoW	87.0	95.2	71.4	93.8	81.2	100.0	75.0	100.0
gl	88.2	71.4	86.7	81.2	95.0	73.1	40.0	66.7
junqiangchen	72.4	100.0	53.3	100.0	75.0	92.3	8.6	100.0
IWM	90.9	95.2	nan	0.0	84.6	84.6	nan	0.0
NexToU	91.3	100.0	93.8	93.8	77.4	92.3	100.0	100.0
NIC-VICOROB-1	86.4	90.5	65.2	93.8	86.2	96.2	50.0	33.3
NIC-VICOROB-2	64.5	95.2	54.2	81.2	71.0	84.6	7.7	33.3
Organizers	91.3	100.0	75.0	93.8	83.9	100.0	50.0	66.7
refrain	87.5	100.0	100.0	93.8	83.3	96.2	100.0	100.0
WilliWillsWissen	91.3	100.0	100.0	93.8	83.3	96.2	nan	0.0

the CoW variants, the predicted segmentation must satisfy strict connectivity and neighborhood conditions without any topological mistakes. The 3rd-A2 anterior variant and with-both-Pcom posterior variant were not matched well by most winning teams with at best 33% matched. Some CoW variants had good topology matching by predicted segmentations: 74% with-Acom anterior variant were matched; 67% to 75% of R-Pcom-only posterior variant were matched; 62% to 82% no-Pcom posterior variant were matched. Team ‘WilliWillsWissen’ had the best topology matching performance by obtaining the highest match ratio in most variants.

We remark on the strict requirements to get a match in our topology matching analysis. Not only do the predicted segmentation need to fulfil the connection conditions with relevant neighbouring CoW components, the segmentation also cannot have topological mistakes in connectivity, fragmentation, or crossover. Thus it was not trivial to get a true positive (TP) in topology matching as reported in Fig. 11. Topology matching is also a more advanced and stringent metric than detection, as it incorporates the detection performance in its evaluation. For example, teams ‘NexToU’ and ‘refrain’ had 100% recall and precision for 3rd-A2 variant in the detection performance for MRA modality, but their topology matching performance were much lower at 0% to 33%. Another example can be seen that winning teams in general had around 90% precision and recall for detecting the Acom, but the anterior variant topology matching for with-Acom and without-Acom variants had much lower match rates at 44% to 74%.

5. Discussions

5.1. Characteristics of the Winning Algorithms

Table 7 shows some key characteristics of the winning algorithms. We identify the following themes from the winning strategies:

- **Train with both modalities can help:** Two winning teams ‘WilliWillsWissen’ and ‘Organizers’ made use of both modalities in the training: Team ‘WilliWillsWissen’ trained their modality-agnostic model with both CTA and MRA modalities in a common pool; Team ‘Organizers’ used both modalities for data augmentation.
- **3D data as default:** Computational cost did not seem to be an obstacle anymore for 3D data, as the winning teams were all 3D deep learning models.
- **Data augmentation:** Data augmentation is offered by default from nnUNet and used by all winning teams. Additional data augmentation was designed in team ‘Organizers’ by registering both modalities. However, it is important to turn off the mirror augmentation in nnUnet for multiclass segmentation to avoid left and right labels being wrongly flipped such as in some predictions by team ‘sjtu.eiee.2-426lab’ as we have seen in Fig. 8.
- **Provided CoW ROI vs custom ROI:** Although we provided the CoW ROI as part of the annotation, it looked like the provided CoW ROI was not particularly useful for algorithm design as the winning teams either did not involve ROI or set up a custom ROI localization and cropping scheme.

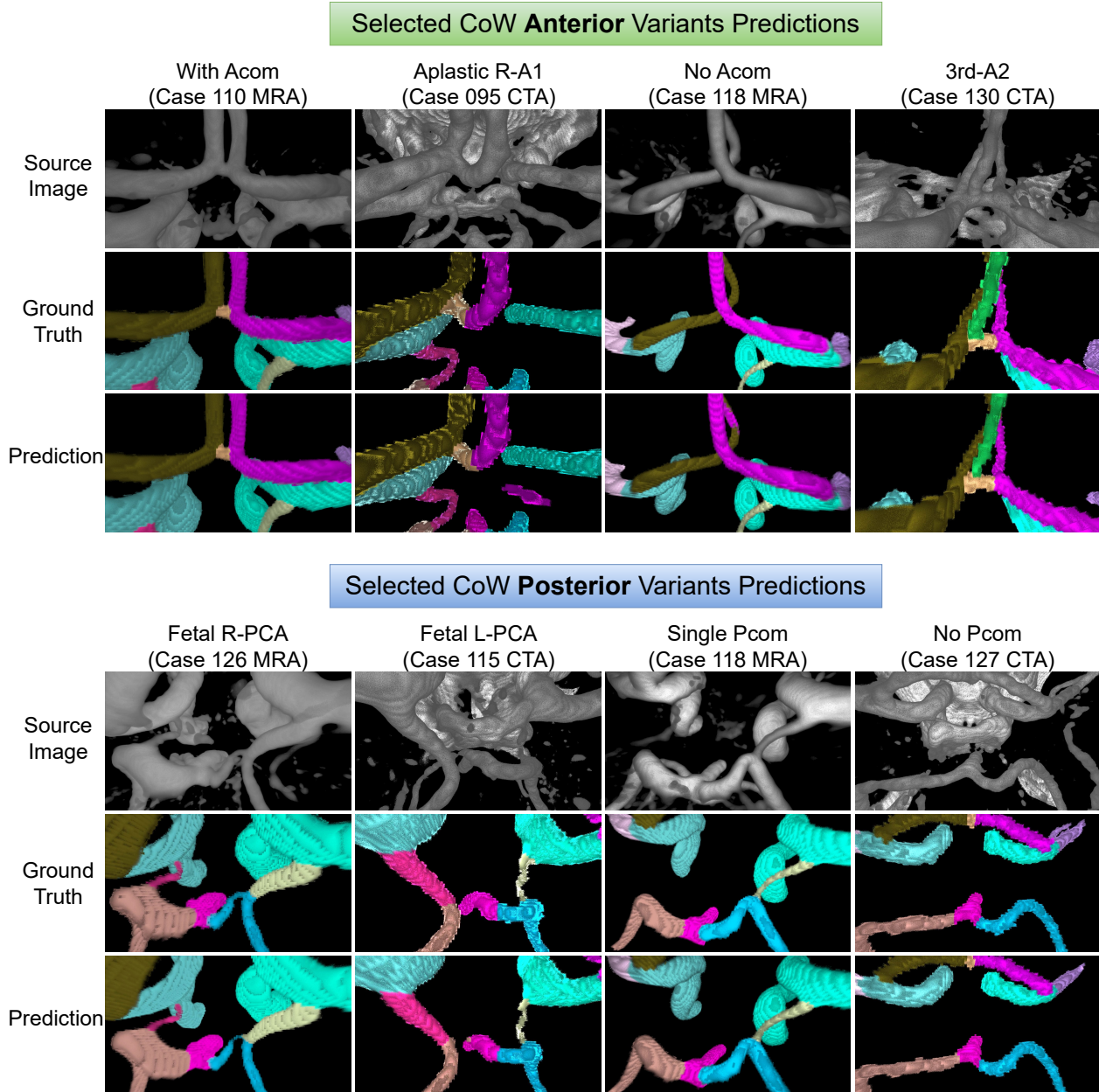


Fig. 10. Qualitative results for anterior (top sub-figure) and posterior (bottom sub-figure) variants in multiclass segmentation task. The predictions are by team ‘WilliWillsWissen’. Various patients are selected. Alternating columns showcasing MRA and CTA.

- **All winning teams used nnUNet:** Winning teams used nnUNet as the basis of the architecture or used it along with other custom architecture setup.
- **Ensemble helps:** Ensembling is offered by default by nnUNet and most winning teams kept the ensembling feature. Team ‘WilliWillsWissen’ carried out additional ensembling for as long as the docker run time limit (15 minutes) allowed.
- **Topological optimizations:** Two winning teams ‘WilliWillsWissen’ and ‘NexToU’ employed methods for topological objects of interest such as the skeletons and centerlines of the vessels. These topology optimizations seemed to improve connectivity, as these two teams had low β_0 errors in multiclass segmentation results. These two teams

also had fewer topological mistakes as seen in the qualitative results, such as fewer intertwined crossover of ACAs or broken fetal R-PCA for Case 126.

5.2. What Has Been Solved?

On a high level, we remark that the validity of framing the CoW characterization problem as a multiclass segmentation task has been demonstrated in this challenge. This general direction of extracting detection and topology for CoW from segmentation showed promises of solving the downstream clinical problems.

As one of the first challenges to have used VR generated annotations, we believe this challenge has successfully shown that VR-based annotation/verification workflow can overcome the

	CoW Anterior Variants Topology Matched (%)						CoW Posterior Variants Topology Matched (%)							
	L-ACA Acom R-ACA		L-ACA R-ACA		L-ACA 3rd-A2 Acom R-ACA		L-Pcom R-Pcom L-PCA BA R-PCA		R-Pcom L-PCA BA R-PCA		L-Pcom L-PCA BA R-PCA		L-PCA BA R-PCA	
	MRA (n=23)	CTA (n=23)	MRA (n=9)	CTA (n=9)	MRA (n=3)	CTA (n=3)	MRA (n=13)	CTA (n=9)	MRA (n=8)	CTA (n=9)	MRA (n=3)	CTA (n=4)	MRA (n=11)	CTA (n=13)
NexToU	61%	70%	22%	67%	33%	0%	15%	33%	38%	22%	33%	50%	82%	54%
Organizers	61%	52%	22%	33%	0%	33%	15%	11%	50%	11%	67%	50%	55%	23%
refrain	65%	-	33%	-	0%	-	8%	-	50%	-	0%	-	64%	-
sjtu_eiee_2-426lab	-	52%	-	22%	-	0%	-	11%	-	11%	-	0%	-	38%
WilliWillsWissen	74%	74%	44%	44%	0%	33%	31%	33%	75%	67%	67%	50%	82%	62%

Fig. 11. CoW variant topology matching performance from top teams in terms of the percentage a particular variant is correctly matched in its topology by the predicted multiclass segmentation masks. A segmentation prediction is counted as a match only if the extracted topology matches the ground-truth's. Highest match ratio for each variant is highlighted in gold color.

Table 7. Key characteristics of the winning algorithms. Colored circles in *Awards* represent first (gold), second (silver) and third (bronze) prizes a team has won in the challenge. Abbreviations: resolution (res), binary (bin) or multiclass (mul) segmentation (seg), localization and extraction of custom ROI (ROI crop), Cross-Entropy (CE), intersection over union (IoU), centerline-boundary Dice (cb-Dice), binary topological interaction (BTI), skeleton recall (SkelRecall).

Team	Awards	Input requiring paired modalities	Training using both modalities	Additional data used	3D data used	Data augmentation	CoW ROI used	# Stages	Multi-stage	Architectures	Loss function	Ensemble	Topological optimizations
NexToU	●●				✓	✓		2	low-res bin seg + full-res seg	nnUNet; NexToU	Dice + CE + cb-Dice + BTI	✓	cb-Dice, BTI
NIC-VICOROB-1	●●				✓	✓		1-2	bin seg + mul seg	nnUNet	Dice + CE	✓	
Organizers	●●		✓		✓	✓	custom	2	ROI crop + seg	nnDetection; nnUNet	CE + IoU; Dice + CE	✓	
refrain	●				✓	✓	custom	2	ROI crop + seg	nnUNet	Dice		
sjtu_eiee_2-426lab	●●				✓	✓	custom	2	ROI crop + seg	nnUNet	Dice + CE		
UW	●				✓	✓		1		nnUNet	Dice + CE + TopK	✓	
WilliWillsWissen	●●		✓		✓	✓		1		nnUNet	Dice + CE + cIDice + SkelRecall	✓	cIDice, skeleton recall

otherwise too time-consuming annotation process on a complex multiclass anatomical segmentation problem. The depth dimension as viewed in 3D in VR offered efficient and powerful annotation/verification capabilities, which proved to be uniquely suitable for curvilinear structures like the CoW vessels that can have complicated spatial orientations and relations among the windy tubes. Without VR, we would not have been able to prepare our multiclass segmentation annotations or the 3D bounding boxes for the CoW anatomy.

As mentioned in the introduction, there has been almost no annotated CoW dataset or CoW labeling software for the CTA modality. Despite the imaging differences in CTA modality (such as more veins and less detailed brain soft tissues visualized), TopCoW challenge has shown that multiclass segmentation models could work equally well for CTA.

The binary segmentation task for CoW merged vessels was predicted by top submissions at above 92% Dice scores, above 97% cIDice scores, and below 0.6 β_0 errors. Although there were some subtle topological mistakes as seen in the qualitative results, the binary segmentation task could be deemed as sufficiently solved.

The bigger and almost always present components of the CoW such as the BA, PCA, ICA, MCA, and ACA (or Group 1 components as we have coined the term earlier) were segmented by top teams at around 85 – 95% Dice scores with a low β_0 errors of less than 0.1. These Group 1 CoW components from the multiclass segmentation task were reasonably solved.

Detection of Pcoms and Acom achieved recall and precision of around 80%–100%. If the goal is to roughly characterize the CoW with presence of communicating arteries like Pcoms and Acom, then the existing winning algorithms can already help to give a fairly decent estimate.

Certain CoW variants such as the with-Acom anterior variant, R-Pcom-only posterior variant, and the no-Pcom posterior variant already could be topology-matched correctly by the predicted segmentation at above ~ 70% rate. Given the strict requirements to get a true positive in a match in topology, these CoW variants could already be characterized by the predicted segmentation quite accurately.

5.3. Open Problems

The CoW component from Group 2 (the communicating arteries and the rare 3rd-A2) were only segmented at around 50–70% Dice scores with higher β_0 errors than Group 1. From the segmentation metrics, these smaller and not-always-present Group 2 CoW components have rooms for improvement.

Topologically, the Group 2 components could be wrongly detected with false positive and false negative, which would interfere with the CoW architecture analysis downstream. More importantly, there could still be topological mistakes for both Group 1 and 2 CoW components. These topological errors could be fragmented vessels or crossover of nearby vessels. We identified the following scenarios more prone to topological mistakes:

- Thin vessel segments with diameters around 1 mm or thinner. We observed that when the diameter of the vessel was near the lower bound of the CoW vessel diameters of around 1 mm (Krabbe-Hartkamp *et al.*, 1998) or thinner, these vessels were often segmented with broken fragments or were wrongly detected.
- When left and right ACAs were tangled or touching, there tended to be crossover between L-ACA and R-ACA.
- Often in fetal PCA variant, Pcom segment could cross over to PCA, especially to the thin P1 segment.

More importantly, many of the CoW variants had a low match rate in the topology by the predicted segmentation. This affects the ability of the segmentation to accurately characterize the topology of the CoW vasculature. It is still an open problem to have a segmentation algorithm that can retain and match the CoW variant topology accurately.

5.4. Limitations and Future Work

We excluded certain rare variants of CoW in our dataset. We can expand the multiclass labels to include and annotate the other rare CoW variants in our dataset, which will make the trained model applicable and more robust to a broader range of the population.

The inter-rater agreement was not analyzed in terms of CoW variant diagnosis, such the detecting CoW components and classifying the CoW variant topology. We analyzed the inter-rater agreement in terms of voxel-wise annotations of individual CoW components after the CoW variant had been diagnosed and verified by the clinicians. Diagnosing the CoW variant can be an expert task that requires considerable highly-specialized clinical experience and knowledge. It is an important future work to quantify the level of agreement among specialized clinical experts for CoW component detection and variant topology classification.

We performed the prevalence and topology matching analysis on a few representative CoW anterior and posterior variants. These selected variants analyzed can be further sub-divided into finer variant types such as whether the A1 segment of ACA or P1 segment of PCA is hypoplastic or aplastic, as done in our prior clinical study (Westphal *et al.*, 2021).

The topological analysis on detection and topology matching was only done post-challenge. The in-challenge leaderboard ranked the submissions based largely on volumetric metrics without in-depth metrics on topological properties. The in-challenge metrics turned out to be inadequate to guide the submissions to preserve the topology of the CoW variants. In the future, our challenge can include direct evaluations on the topologies of the predicted segmentation, such as the connection conditions with relevant neighbouring CoW components.

The Group 2 CoW components are smaller in diameter and volume, which are not best evaluated in overlap-based metrics like Dice and cIDice scores as they are sensitive to small disagreement in voxels (Reinke *et al.*, 2021). In the future, boundary-based metrics like Hausdorff distance can be used for CoW components with smaller structure size.

5.5. Clinical Potential

Lastly, we highlight the clinical potential of this challenge. One of the main motivations of this challenge is to meet the clinical demand for an efficient software tool to analyze the angio-architecture of the CoW, which does not yet exist in clinical practice.

Neurologists can potentially use such an automated CoW characterization tool to screen patients and healthy controls for vascular risk factors for stroke and aneurysm. The primary collaterals (at the level of the CoW) and the CoW configurations have been hypothesized to affect the severity of stroke (Liebeskind, 2003; Chuang *et al.*, 2013; van Seeters *et al.*, 2015) and aneurysm formation (Rinaldo *et al.*, 2016), which can now be analyzed at scale with an automated screening tool for CoW.

Neuro- and neurointerventional-surgeons can use the CoW segmentation tool to reduce the cognitive workload and more quickly identify principal and communicating cerebral arteries, which can potentially help with surgical planning and diagnosis.

Clinical education and training can also benefit from such an automated CoW segmentation tool, which can provide consistent and quality anatomical labeling of the CoW to those without access to highly-trained clinical experts.

Finally, the CoW characterization software works on an individual level, thus offers personalized assessment and treatment planning for patients with neurovascular diseases.

6. Conclusion

TopCoW 2023 challenge attracted over 140 registered participants from four continents, which resulted in 18 high-quality submitted algorithms. The binary segmentation task for CoW vessels was sufficiently solved. The more challenging multiclass CoW anatomical segmentation task was also partially solved with good results on many CoW components. Certain CoW components that are not always present such as the communicating arteries and the 3rd-A2 had lower metric results. Additional topological analysis for detection and topology matching was done for the multiclass segmentation predictions. Presence/absence of CoW components could already be detected reasonably well. But the topology extracted from the

predicted segmentation could not match as accurately for some CoW variants. There is still room for improvement for the segmentation to retain and match the CoW variants topologically.

Being the first challenge to attempt the CoW multiclass anatomical segmentation task, TopCoW has demonstrated the potential of tackling the CoW characterization problem via segmentation. TopCoW released the first dataset on paired CTA and MRA with annotations, thus enabled some of the first anatomical segmentation models for CoW, especially for the CTA modality. TopCoW was the first challenge to use a VR-based annotation workflow, which was crucial in preparing the multiclass annotations. As a first benchmark for such a CoW segmentation task, TopCoW gathered strong baseline results for further algorithm development and comparison.

Ultimately we want to solve real clinical problems, and one of them is to prototype an automated CoW characterization tool for diagnosis, screening, and treatment. An accurate characterization of the CoW is of great clinical relevance, and we hope TopCoW challenge has piqued the interest of the community on this worthwhile endeavour.

Appendix A. Submitted Algorithms and Method Descriptions

In this section we briefly summarize the methods and algorithms of all the participating teams ordered alphabetically by team names:

2i_mtl. The submission was made by Emmanuel Montagnon and Laurent Letourneau-Guillon. The team took part in the CT binary task only. They employed a two-stage approach consisting of a patch-based 3D AttentionUNet (Oktay et al., 2018) followed by a 3D autoencoder to mitigate false positives. The autoencoder received as input both an image patch and the AttentionUNet mask prediction.

agaldran. The submissions were made by Adrian Galdran. He took part in all four tracks and task. His approach was based on a self-adapting 3D dynamic UNet provided by the MONAI library. He performed internal cross-validation on the patch size. For the multiclass submissions the Docker containers were defective leading to corrupted results. The code is available upon request.

EURECOM. The submissions were made by Francesco Galati, Daniele Falcetta and Maria A. Zuluaga. They took part in both binary segmentation tasks and applied a single model strategy for multi-domain vessel segmentation. They employed an adapted version of their A2V framework (Galati et al., 2023) consisting of a single encoder-generator architecture for image reconstruction, translation, and ultimately segmentation with a shared latent space for both modalities. In a first step they extracted brain masks required by A2V using SynthSeg (Billot et al., 2023). The code will be made available on github.com/i-vesseg/MultiVesSeg.

gbCoW. The submissions were made by Chaolong Lin and Haoran Zhao. They took part in the MRA binary and multiclass tasks using the nnUNet framework (Isensee et al., 2021) for patch-based 3D segmentation. They trained a single model on the multiclass labels only; the binary masks were obtained from their multiclass predictions. The Docker containers and code will be made publicly available.

gl. The submissions were made by Zehan Zhang. He submitted algorithms to both multiclass segmentation tasks following a multi-step approach consisting of 1) the extraction of a custom ROI using a dataset specific atlas and affine registration, 2) binary segmentation and 3) subsequent multiclass segmentation with a 2-channel input (image ROI and binary mask). For the segmentation both the 3D MedNexT (Roy et al., 2023) and UX-Net (Lee et al., 2022) architectures were employed as an ensemble. The inference code is available on github.com/zzh980123/TopCoW_Algo_Submission.

IWantToGoToCanada. The submissions were made by Sinyoung Ra, Jongyun Hwang and Hyunjin Park. They took part in the CTA binary and multiclass tasks. The nnUNet was used to extract the binary segmentation mask. For the subsequent multiclass segmentation a 3D Swin-UNETR (Hatamizadeh et al., 2021) architecture was employed with both the image and the binary mask as input.

junqiangchen. The submissions were made by Junqiang Chen, taking part in all four tracks and tasks. A two-stage approach was employed using the VNet3D (Milletari et al., 2016) for both stages: In the first stage a custom ROI was extracted based on a binary segmentation, in the second stage the segmentation was performed on the ROI only. The code is available on github.com/junqiangchen/PytorchDeepLearning.

IWM. The submissions were made by Marek Wodzinski and Henning Müller. They took part in all four tracks and tasks using a patch-based 3D ResidualUNet with a focus on data pre-processing and augmentation. The code will be available on github.com/MWod/TopCOW_2023_MW.

NexToU. The submissions were made by Pengcheng Shi, Wei Liu and Ting Ma. They took part in all four tracks and tasks. The nnUNet was used for a first low-res binary segmentation followed by their own NexToU architecture (Shi et al., 2023) for full-res 3D cascading and a final MLP layer for task-specific output. They introduce the novel centerline boundary Dice (cb-Dice) loss function that is both topology aware and diameter balanced. The codebase for NexToU can be found on github.com/PengchengShi1220/NexToU; the cbDice loss function is available on github.com/PengchengShi1220/cbDice.

NIC-VICOROB-1. The submissions were made by Cansu Yalçın, Rachika E. Hamadache, Joaquim Salvi and Xavier Lladó. They took part in all four tracks and tasks using a patch-based 3D nnUNet. Working in two stages with a 2-channel input consisting of both the image and the binary mask improved the segmentation results for both the CTA and MRA multiclass tasks. Due to inference time limitations they could submit this approach only for the CTA multiclass task.

NIC-VICOROB-2. The submissions were made by Uma Maria Lal-Trehan Estrada, Valeriia Abramova, Luca Giancardo and Arnau Oliver, taking part in all four tracks and tasks. For the binary segmentation tasks they employed a patch-based 3D AttentionUNet. For the multiclass segmentation tasks they employed a two-stage approach using a 2D AttentionUNet with full axial slices and binary segmentation masks, obtained from the 3D AttentionUNet, as input. The 2D approach was chosen due to GPU memory limitations. The code and Docker images are available upon request.

Organizers. The submissions were made by the two Top-CoW organizers Fabio Musio and Kaiyuan Yang. They took part in the multiclass tasks of both tracks using a two-stage approach: The nnDetection framework was used to detect and extract custom ROIs based on the binary labels and a 3D nnUNet was employed for the subsequent multiclass segmentation on the ROIs. Additionally, inter-modal registration was used as a data augmentation strategy, registering all the image pairs and thereby doubling the size of the training set for both modalities. The code will be available on github.com/fmusio/TopCoWSubmissions.

refrain. The submissions were made by Jialu Liu, Haibin Huang and Yue Cui. They submitted algorithms for the MRA binary and multiclass task, employing a 3D nnUNet for both tasks. A template atlas was used to extract a custom ROI via registration. Furthermore, they used data augmentation to balance the training set with respect underrepresented CoW variants and applied segment specific loss weighting with higher weights for R-Pcom, L-Pcom, Acom and 3rd-A2. The code is available on github.com/Vessel-Segmentation/Topcow_private.

sjtu_eiee_2-426lab. The submissions were made by Zehang Lin, Yusheng Liu and Shunzhi Zhu, taking part in the CTA binary and multiclass tasks. They used a two-stage approach using the 3D nnUNet: A first binary segmentation for a custom ROI extraction followed by a segmentation on the extracted ROI only.

UB-VTL. The submissions were made by Tatsat R. Patel and Vincent M. Tutino. They took part in both binary segmentation tasks employing a patch-based 3D Brave-Net (Hilbert et al., 2020) taking as input a normal patch and a low-res patch for more context. As modifications the authors added residual connections, used parametric rectified linear units (PReLU) as activations and worked with the centerline Dice (clDice) (Shit et al., 2021) as a loss function. The code will be made available on github.com/tatsatra/TopCowCTBinary.

UW. The submission was made by Maysam Orouskhani, Huayu Wang, Mahmud Mossa-Basha and Chengcheng Zhu. They took part in the MRA binary task using the patch-based 3D nnUNet framework with a modified 3-component loss function consisting of Dice, Cross-Entropy (CE) and TopK loss. The code, models and trained weights can be accessed via github.com/orouskhani/TopCow2023.

WilliWillsWissen. The submissions were made by Maximilian R. Rokuss, Yannick Kirchhoff, Nico Disch, Julius Holzschuh, Fabian Isensee and Klaus Maier-Hein. The team took part in all four tracks and tasks employing a patch-based 3D nnUNet with various adaptations. To improve connectedness they incorporated the clDice and a recall on the skeleton of the vessels (SkelRecall) (Kirchhoff et al., 2024); they trained the models on all available data, irrespective of the modality; and they employed a 5-fold cross-validation ensemble per model as well as a subsequent ensemble of two differently trained models for each submission. The Docker can be accessed upon request and the code will be made publicly available.

ysato. The submission was made by Yuki Sato, taking part in the MRA binary task. The author employed a non-deep learning approach based on recursive algorithm consisting of auto vessel thresholding and region growing with a rule-based automated seed point selection. It was the only non-deep learning based submission to our challenge. Accordingly, the inference time per case was very short (~15s) and the computations could be done on a CPU.

Appendix B. Multiclass Segmentation Task Results with Per Case Class-Average

Table B.8 shows the results of the multiclass segmentation task for the MRA and CTA tracks as used for our public leaderboards on grand-challenge. The results for Dice scores and β_0 errors were computed for each class separately and class-average was taken per case.

Appendix C. Characteristics of All Submissions

In Table C.9 we summarize the key characteristics for each participating team.

Data Availability

The training and validation data can be accessed on the challenge website, as described in the paper.

Code Availability

The implementation of our evaluation metric code is open sourced at https://github.com/CoWBenchmark/TopCoW_Eval_Metrics.

See Appendix A for individual team’s open sourced code.








Acknowledgments

The challenge is supported by the Digitalization Initiative of the Zurich Higher Education Institutions (DIZH) and the Helmut Horten Foundation. We thank Hrvoje Bogunović and Amrish Soundararajan for helpful discussions and suggestions before the proposal. We also thank Nathan Spencer and Michael Morehead from syGlass for the technical assistance for the

Table B.8. Results (mean \pm standard deviation) of the multiclass segmentation tasks for MRA and CTA in terms of class average Dice scores, centerline Dice (cDice) scores and class average errors in the zero-th Betti number β_0 . The cDice scores are computed on the merged binary class, the Dice scores and β_0 errors are computed for each class separately and the average is taken per case. The arrow indicates the favorable direction. The top three values for each metric and each track are marked as gold, silver and bronze cells in decreasing order. If a team only submitted to one of the tracks the columns of the other track are filled with a '-'. The winning team names are in bold.

Team	Multi-Class segmentation performance					
	MRA			CTA		
	Per case class-average Dice (%) \uparrow	cDice (%) \uparrow	Per case class-average β_0 error \downarrow	Per case class-average Dice (%) \uparrow	cDice (%) \uparrow	Per case class-average β_0 error \downarrow
agaldran	0.01 \pm 0.07	0.16 \pm 0.69	1.01 \pm 0.18	0.15 \pm 0.66	0.77 \pm 1.62	1.07 \pm 0.32
gbCoW	80.51 \pm 14.69	98.10 \pm 2.33	0.28 \pm 0.27	-	-	-
gl	81.27 \pm 9.16	95.81 \pm 5.11	0.09 \pm 0.08	54.02 \pm 21.76	75.80 \pm 28.05	0.24 \pm 0.22
IWantToGoToCanada	-	-	-	74.34 \pm 7.90	97.61 \pm 1.78	0.77 \pm 0.50
junqiangchen	71.56 \pm 9.72	96.86 \pm 2.80	0.87 \pm 0.41	67.68 \pm 5.97	95.91 \pm 1.63	1.09 \pm 0.37
IWM	79.03 \pm 8.75	96.23 \pm 3.11	0.27 \pm 0.22	72.49 \pm 8.46	92.78 \pm 5.13	0.32 \pm 0.19
NexToU	83.76 \pm 6.95	97.29 \pm 2.29	0.14 \pm 0.14	81.67 \pm 6.81	97.78 \pm 1.88	0.16 \pm 0.14
NIC-VICOROB-1	77.13 \pm 20.15	96.31 \pm 5.78	0.11 \pm 0.09	51.84 \pm 31.11	97.86 \pm 2.38	0.43 \pm 0.38
NIC-VICOROB-2	65.99 \pm 8.76	94.12 \pm 6.12	2.64 \pm 3.00	62.41 \pm 8.22	95.65 \pm 3.38	2.31 \pm 1.37
Organizers	83.98 \pm 7.33	98.06 \pm 2.30	0.16 \pm 0.13	77.00 \pm 11.95	96.98 \pm 3.48	0.23 \pm 0.26
refrain	83.72 \pm 5.79	98.20 \pm 1.84	0.19 \pm 0.17	-	-	-
sjtu_eiee_2-426lab	-	-	-	67.46 \pm 27.78	97.15 \pm 3.22	0.23 \pm 0.27
WilliWillsWissen	84.58 \pm 6.47	97.21 \pm 3.37	0.06 \pm 0.06	83.32 \pm 5.65	98.12 \pm 1.86	0.11 \pm 0.11

Table C.9. Key characteristics of all submitted algorithms. The winning team names are in bold. Colored circles in Awards represent first (gold), second (silver) and third (bronze) prizes a team has won in the challenge. Abbreviations: false positive (FP), extraction of brain mask (brain extract), resolution (res), binary (bin) or multiclass (mul) segmentation (seg), localization and extraction of custom ROI (ROI crop), Cross-Entropy (CE), intersection over union (IoU), centerline-boundary Dice (cb-Dice), binary topological interaction (BTI), skeleton recall (SkelRecall), region growing (grow).

Team	Awards	Input requiring paired modalities	Training using both modalities	Additional data used	3D data used	Data augmentation	CoW ROI used	# Stages	Multi-stage	Architectures	Loss function	Ensemble	Topological components
2i_mtl					\checkmark	\checkmark	provided	2	seg + reduce FP	AttentionUNet; Autoencoder	Dice + focal; MSE		
agaldran					\checkmark	\checkmark		1		DynUNet	CE	\checkmark	
EURECOM			\checkmark				provided	2	brain extract + seg	SynthSeg; A2V	Dice + CE		
gbCoW					\checkmark			1		nnUNet	Dice + CE	\checkmark	
gl					\checkmark	\checkmark	custom	3	ROI crop + bin seg + mul seg	MedNexT/UX-Net	Dice + CE	\checkmark	
IWantToGoToCanada					\checkmark	\checkmark		2	bin seg + mul seg	nnUNet; Swin-UNETR	Dice + CE; Dice + Focal	\checkmark	
junqiangchen					\checkmark	\checkmark	custom	2	ROI crop + seg	VNet3D	Dice + CE		
IWM					\checkmark	\checkmark		1		ResUNet	Dice + Focal		
NexToU					\checkmark	\checkmark		2	low-res bin seg + full-res seg	nnUNet; NexToU	Dice + CE + cb-Dice + BTI	\checkmark	cb-Dice, BTI
NIC-VICOROB-1					\checkmark	\checkmark		1 - 2	bin seg + mul seg	nnUNet	Dice + CE	\checkmark	
NIC-VICOROB-2							provided	1 - 2	bin seg + mul seg	AttentionUNet	Focal		
Organizers			\checkmark		\checkmark	\checkmark	custom	2	ROI crop + seg	nnDetection; nnUNet	CE + IoU; Dice + CE	\checkmark	
refrain					\checkmark	\checkmark	custom	2	ROI crop + seg	nnUNet	Dice		
sjtu_eiee_2-426lab					\checkmark	\checkmark	custom	2	ROI crop + seg	nnUNet	Dice + CE		
UB-VTL					\checkmark		provided	1		Brave-Net	cDice		cDice
UW					\checkmark	\checkmark		1		nnUNet	Dice + CE + TopK	\checkmark	
WilliWillsWissen			\checkmark		\checkmark	\checkmark		1		nnUNet	Dice + CE + cDice + SkelRecall	\checkmark	cDice, skeleton recall
ysato					\checkmark			2	threshold + grow				

VR setup, and James Meakin and Chris van Run from grandchallenge.org for the technical support for the challenge infrastructure.

Team **2i_mtl** was supported by Grants from the Quebec Bio-Imaging Network (Project No. 21.24) and start-up funds from the Centre de Recherche du CHUM and Departement de radiologie, radio-oncologie et medecine nucleaire, Universite de Montreal/Bayer. Laurent Letourneau-Guillon is supported by a Clinical Research Scholarship–Junior 1 Salary Award (311203)

from the Fonds de Recherche du Quebec en Sante and Fondation de l'Association des Radiologistes du Quebec. Team **agaldran** Adrian Galdran was funded by a Marie Skłodowska-Curie Fellowship (No. 892297). Team **EURECOM** was partially funded by the French government, through the 3IA Cote d'Azur Investments in the Future project managed by the ANR (ANR-19-P3IA-0002) and by the ANR JCJC project I-VESEGG (22-CE45-0015-01). Team **IWantToGoToCanada** was supported by the National Research Foundation (NRF-

2020M3E5D2A01084892), Institute for Basic Science (IBS-R015-D1), ITRC support program (IITP-2023-2018-0-01798), AI Graduate School Support Program (2019-0-00421), ICT Creative Consilience program (IITP-2023-2020-0-01821), and the Artificial Intelligence Innovation Hub program (2021-0-02068). Team **IWM** wants to acknowledge the Polish HPC infrastructure PLGrid support (No. PLG/2023/016239). Team **NIC-VICOROB-1** was supported by the Ministerio de Ciencia e Innovacion (DPI2020-114769RB-I00) as well as by ICREA under the ICREA Academia programme. Team **NIC-VICOROB-2** was also partly supported the Ministerio de Ciencia e Innovacion (DPI2020-114769RB-I00). Team **UB-VTL** wants to acknowledge the computational resources provided by the Center of Computational Research (CCR) at University of Buffalo. Team **UW** was supported by the United States National Institute of Health (grants R01HL162743 and R00HL136883). Team **WilliWillsWissen** was supported by the Helmholtz Association under the joint research school “HIDSS4Health – Helmholtz Information and Data Science School for Health” and part of their work was funded by Helmholtz Imaging (HI), a platform of the Helmholtz Incubator on Information and Data Science.

References

- Banga, P.V., Varga, A., Csobay-Novák, C., Kolossváry, M., Szántó, E., Oderich, G.S., Entz, L., Sótonyi, P., 2018. Incomplete circle of willis is associated with a higher incidence of neurologic events during carotid eversion endarterectomy without shunting. *Journal of Vascular Surgery* 68, 1764–1771.
- Billot, B., Greve, D., Puonti, O., Thielscher, A., Van Leemput, K., Fischl, B., Dalca, A., Iglesias, J., 2023. Synthseg: Segmentation of brain mri scans of any contrast and resolution without retraining. *Medical Image Analysis* 86, 102789.
- Bogunović, H., Pozo, J.M., Cárdenes, R., San Román, L., Frangi, A.F., 2013. Anatomical labeling of the circle of willis using maximum a posteriori probability estimation. *IEEE Transactions on Medical Imaging* 32, 1587–1599.
- Bouthillier, A., Van Loveren, H.R., Keller, J.T., 1996. Segments of the internal carotid artery: a new classification. *Neurosurgery* 38, 425–433.
- Bullitt, E., Zeng, D., Gerig, G., Aylward, S., Joshi, S., Smith, J.K., Lin, W., Ewend, M.G., 2005. Vessel tortuosity and brain tumor malignancy: a blinded study. *Academic Radiology* 12, 1232–1240.
- Chen, L., Hatsukami, T., Hwang, J.N., Yuan, C., 2020. Automated intracranial artery labeling using a graph neural network and hierarchical refinement, in: *Medical Image Computing and Computer Assisted Intervention—MICCAI 2020: 23rd International Conference, Lima, Peru, October 4–8, 2020, Proceedings, Part VI* 23, Springer. pp. 76–85.
- Chuang, Y.M., Chan, L., Lai, Y.J., Kuo, K.H., Chiou, Y.H., Huang, L.W., Kwok, Y.T., Lai, T.H., Lee, S.P., Wu, H.M., et al., 2013. Configuration of the circle of willis is associated with less symptomatic intracerebral hemorrhage in ischemic stroke patients treated with intravenous thrombolysis. *Journal of Critical Care* 28, 166–172.
- Dumais, F., Caceres, M.P., Janelle, F., Seifeldine, K., Arès-Bruneau, N., Gutierrez, J., Boci, C., Whittingstall, K., 2022. eicab: A novel deep learning pipeline for circle of willis multiclass segmentation and analysis. *NeuroImage* 260, 119425.
- Galati, F., Falcetta, D., Cortese, R., Casolla, B., Prados, F., Burgos, N., Zuluaga, M.A., 2023. A2v: A semi-supervised domain adaptation framework for brain vessel segmentation via two-phase training angiography-to-venography translation. *arXiv preprint arXiv:2309.06075*.
- Hatamizadeh, A., Nath, V., Tang, Y., Yang, D., Roth, H.R., Xu, D., 2021. Swin unet: Swin transformers for semantic segmentation of brain tumors in mri images, in: *International MICCAI BrainLesion Workshop*, Springer. pp. 272–284.
- Hilbert, A., Madai, V.I., Akay, E.M., Aydin, O.U., Behland, J., Sobesky, J., Galinovic, I., Khalil, A.A., Taha, A.A., Wuerfel, J., et al., 2020. Brave-net: fully automated arterial brain vessel segmentation in patients with cerebrovascular disease. *Frontiers in artificial intelligence* 3, 552258.
- Hong, S.W., Song, H.N., Choi, J.U., Cho, H.H., Baek, I.Y., Lee, J.E., Kim, Y.C., Chung, D., Chung, J.W., Bang, O.Y., et al., 2023. Automated in-depth cerebral arterial labelling using cerebrovascular vasculature reframing and deep neural networks. *Scientific Reports* 13, 3255.
- Iqbal, S., 2013. A comprehensive study of the anatomical variations of the circle of willis in adult human brains. *Journal of Clinical and Diagnostic Research: JCDR* 7, 2423.
- Isensee, F., Jaeger, P.F., Kohl, S.A., Petersen, J., Maier-Hein, K.H., 2021. nnu-net: a self-configuring method for deep learning-based biomedical image segmentation. *Nature Methods* 18.
- Isensee, F., Schell, M., Pflueger, I., Brugnara, G., Bonekamp, D., Neuberger, U., Wick, A., Schlemmer, H.P., Heiland, S., Wick, W., et al., 2019. Automated brain extraction of multisequence mri using artificial neural networks. *Human Brain Mapping* 40, 4952–4964.
- Kaltenecker, D., Al-Maskari, R., Negwer, M., Hoehner, L., Kofler, F., Zhao, S., Todorov, M., Rong, Z., Paetzold, J.C., Wiestler, B., Piraud, M., Rueckert, D., Geppert, J., Morigny, P., Rohm, M., Menze, B.H., Herzig, S., Berriel Diaz, M., Ertürk, A., 2024. Virtual reality-empowered deep-learning analysis of brain cells. *Nature Methods*, 1–10.
- Kim, K.M., Kang, H.S., Lee, W.J., Cho, Y.D., Kim, J.E., Han, M.H., 2016. Clinical significance of the circle of willis in intracranial atherosclerotic stenosis. *Journal of Neurointerventional Surgery* 8, 251–255.
- Kirchhoff, Y., Rokuss, M.R., Roy, S., Kovacs, B., Ulrich, C., Wald, T., Zenk, M., Vollmuth, P., Kleesiek, J., Isensee, F., et al., 2024. Skeleton recall loss for connectivity conserving and resource efficient segmentation of thin tubular structures. *arXiv preprint arXiv:2404.03010*.
- Krabbe-Hartkamp, M.J., Van der Grond, J., De Leeuw, F., de Groot, J.C., Algra, A., Hillen, B., Breteler, M., Mali, W., 1998. Circle of willis: morphologic variation on three-dimensional time-of-flight mr angiograms. *Radiology* 207, 103–111.
- Lee, H.H., Bao, S., Huo, Y., Landman, B.A., 2022. 3d ux-net: A large kernel volumetric convnet modernizing hierarchical transformer for medical image segmentation. *arXiv preprint arXiv:2209.15076*.
- Li, X., Morgan, P.S., Ashburner, J., Smith, J., Rorden, C., 2016. The first step for neuroimaging data analysis: Dicom to nifti conversion. *Journal of Neuroscience Methods* 264, 47–56.
- Liebeskind, D.S., 2003. Collateral circulation. *Stroke* 34, 2279–2284.
- Menten, M.J., Paetzold, J.C., Zimmer, V.A., Shit, S., Ezhov, I., Holland, R., Probst, M., Schnabel, J.A., Rueckert, D., 2023. A skeletonization algorithm for gradient-based optimization, in: *Proceedings of the IEEE/CVF International Conference on Computer Vision (ICCV)*, pp. 21394–21403.
- Milletari, F., Navab, N., Ahmadi, S.A., 2016. V-net: Fully convolutional neural networks for volumetric medical image segmentation, in: *2016 fourth International Conference on 3D Vision (3DV)*, IEEE. pp. 565–571.
- Oktay, O., Schlemper, J., Folgoc, L.L., Lee, M., Heinrich, M., Misawa, K., Mori, K., McDonagh, S., Hammerla, N.Y., Kainz, B., et al., 2018. Attention u-net: Learning where to look for the pancreas. *arXiv preprint arXiv:1804.03999*.
- Osborn, A.G., 2013. *Osborn’s Brain: Imaging, Pathology, and Anatomy*. Amirsys.
- Pidhorskyi, S., Morehead, M., Jones, Q., Spirou, G., Doretto, G., 2018. sy-Glass: Interactive exploration of multidimensional images using virtual reality head-mounted displays. *arXiv preprint arXiv:1804.08197*.
- Reinke, A., Tizabi, M.D., Sudre, C.H., Eisenmann, M., Rädtsch, T., Baumgartner, M., Acion, L., Antonelli, M., Arbel, T., Bakas, S., et al., 2021. Common limitations of image processing metrics: A picture story. *arXiv preprint arXiv:2104.05642*.
- Rinaldo, L., McCutcheon, B.A., Murphy, M.E., Bydon, M., Rabinstein, A.A., Lanzino, G., 2016. Relationship of a1 segment hypoplasia to anterior communicating artery aneurysm morphology and risk factors for aneurysm formation. *Journal of Neurosurgery* 127, 89–95.
- Robben, D., Sunaert, S., Thijs, V., Wilms, G., Maes, F., Suetens, P., 2013. Anatomical labeling of the circle of willis using maximum a posteriori graph matching, in: *Medical Image Computing and Computer-Assisted Intervention—MICCAI 2013: 16th International Conference, Nagoya, Japan, September 22–26, 2013, Proceedings, Part I* 16, Springer. pp. 566–573.
- Robben, D., Türetken, E., Sunaert, S., Thijs, V., Wilms, G., Fua, P., Maes, F., Suetens, P., 2016. Simultaneous segmentation and anatomical labeling of the cerebral vasculature. *Medical Image Analysis* 32, 201–215.
- Roy, S., Koehler, G., Ulrich, C., Baumgartner, M., Petersen, J., Isensee, F.,

- Jaeger, P.F., Maier-Hein, K.H., 2023. Mednext: transformer-driven scaling of convnets for medical image segmentation. *International Conference on Medical Image Computing and Computer-Assisted Intervention (MICCAI)*, 405–415.
- Schimke, N., Hale, J., 2011. Quickshear defacing for neuroimages, in: *Proceedings of the 2nd USENIX Conference on Health Security and Privacy*, USENIX Association, USA. p. 11.
- van Seeters, T., Hendrikse, J., Biessels, G.J., Velthuis, B.K., Mali, W.P., Kappelle, L.J., van der Graaf, Y., Group, S.S., 2015. Completeness of the circle of willis and risk of ischemic stroke in patients without cerebrovascular disease. *Neuroradiology* 57, 1247–1251.
- Shi, P., Guo, X., Yang, Y., Ye, C., Ma, T., 2023. Nextou: Efficient topology-aware u-net for medical image segmentation. *arXiv preprint arXiv:2305.15911*.
- Shit, S., Paetzold, J.C., Sekuboyina, A., Ezhov, I., Unger, A., Zhylka, A., Pluim, J.P., Bauer, U., Menze, B.H., 2021. *ctDice*-a novel topology-preserving loss function for tubular structure segmentation, in: *Proceedings of the IEEE/CVF Conference on Computer Vision and Pattern Recognition (CVPR)*, pp. 16560–16569.
- Stucki, N., Paetzold, J.C., Shit, S., Menze, B., Bauer, U., 2023. Topologically faithful image segmentation via induced matching of persistence barcodes, in: *International Conference on Machine Learning (ICML)*, PMLR. pp. 32698–32727.
- Vos, I., Ruigrok, Y., Velthuis, B., Kuijf, H., et al., 2023. Crown challenge: Circle of willis intracranial artery classification and quantification challenge 2023. <https://crown.isi.uu.nl/>. Accessed: 2023-10-30.
- Wasserthal, J., Breit, H.C., Meyer, M.T., Pradella, M., Hinck, D., Sauter, A.W., Heye, T., Boll, D.T., Cyriac, J., Yang, S., et al., 2023. Totalsegmentator: Robust segmentation of 104 anatomic structures in ct images. *Radiology: Artificial Intelligence* 5.
- Westphal, L.P., Lohaus, N., Winklhofer, S., Manzolini, C., Held, U., Steigmiller, K., Hamann, J.M., El Amki, M., Dobrocky, T., Panos, L.D., et al., 2021. Circle of willis variants and their association with outcome in patients with middle cerebral artery-m1-occlusion stroke. *European Journal of Neurology* 28, 3682–3691.
- Yang, F., Li, H., Wu, J., Li, M., Chen, X., Jiang, P., Li, Z., Cao, Y., Wang, S., 2017. Relationship of a1 segment hypoplasia with the radiologic and clinical outcomes of surgical clipping of anterior communicating artery aneurysms. *World Neurosurgery* 106, 806–812.